High Power Operation of the In-Band Diode-Pumped $Nd:GdVO_4$ Lasers

by

Mohammad Nadimi

A Thesis submitted to the Faculty of Graduate Studies of
The University of Manitoba
in partial fulfilment of the requirements of the degree of

DOCTOR OF PHILOSOPHY

Department of Electrical and Computer Engineering

University of Manitoba

Winnipeg, Manitoba, Canada

Abstract

The main obstacle in power scaling of the well-known Nd-doped lasers such as Nd:YVO_4 is the thermal lensing effect. One of the proposed solutions to effectively alleviate this problem was based on the reduction of heating within the laser crystal. This was extensively investigated with the Nd:YVO_4 crystal by pumping the laser at 914 nm instead of the standard pumping at 808 nm wavelength. In context of high power applications, the crystal of Nd:$GdVO_4$ is an interesting alternative to the Nd:YVO_4 as it offers the benefits of good spectral features (similar to Nd:YVO_4) and much higher thermal conductivity. However, there is only one proof-of-principle work on continuous-wave (CW) Nd:$GdVO_4$ laser using this pumping approach in which an output power of 3.35 W was reported. The full power scaling potential of the Nd:$GdVO_4$ laser crystal to produce high output power has not been demonstrated to date. In this PhD thesis, I addressed this issue and investigated the high power operation of Nd:$GdVO_4$ lasers under a new pumping wavelength of 912 nm.

First, the thermal lensing behaviour of a 1063 nm Nd:$GdVO_4$ was studied, both experimentally and by finite element analysis (FEA) method. The thermal lensing strength in Nd:$GdVO_4$ laser under 912 nm pumping was significantly reduced when compared to the Nd:$GdVO_4$ laser with 808 nm pumping or even Nd:YVO_4 laser with 914 nm pumping. The next step of this research was focused on high power operation of Nd:$GdVO_4$ lasers where we achieved 19.8 W of output power at 1063 nm.

As a side work in the CW regime of operation, the possibility of discrete wavelength tuning and dual-wavelength operation of the Nd:$GdVO_4$ laser were examined by using an intracavity birefringent filter. Discrete wavelength operation at four different wavelengths was demonstrated.

Furthermore, for the first time we were able to demonstrate a dual-wavelength operation of the Nd:$GdVO_4$ laser as a 1063 and 1071 nm wavelength pair.

The last aspect of this PhD thesis was concentrated on generation of picosecond pulses. We were able to report on the first semiconductor saturable absorber mirror (SESAM) mode-locked (ML) Nd:$GdVO_4$ laser with 912 nm pumping. The laser generated 10.14 W of average output power with the pulse width of 16 ps at the repetition rate of 85.2 MHz. To the best of our knowledge this is the highest average output power ever obtained from any of the SESAM mode-locked Nd-doped solid-state lasers that were pumped around 912 nm.

Acknowledgment

First and foremost, I would like to thank my supervisor, Prof. Arkady Major for giving me the opportunity to join his research group. I deeply appreciate his guidance, support, patience, motivation, and immense knowledge.

I would also like to thank the committee members Prof. Gerald Gwinner and Prof. Cyrus Shafai, not only for the time they spent to review my progress but also for the constructive comments and suggestions on the thesis. I am also deeply appreciative for the time Dr. Ivan Lima spent on reviewing this thesis, and for all the helpful comments he provided.

Special thanks to the associate head of graduate studies Dr. Shaahin Filizadeh and also student advisor Amy Dario for their generous services in the Department of Electrical and Computer Engineering.

I would also like to thank my colleagues S. Manjooran, Dr. R. Akbari, Dr. S. Ghanbari, Dr. V. M. Collado, C. Q. Howlader, M. Anisur and C. Onyenekwu. I learned a lot through fruitful discussions from them. I would also like to express my gratitude to Dr. Tanant Waritanant for his generous help in the laboratory.

I also extend my gratitude to the Natural Sciences and Engineering Research Council of Canada and the University of Manitoba for their financial support.

I am very fortune that I had my kind and wonderful family: my mother, Ameneh, my father, Abdollah and my sister, Somayeh for all of their care and praying.

Keeping the best for the last, I would like to thank my wife, Zohreh for all her love and support during every moment of this journey.

Contents

List of Figures

List of Tables

List of Symbols and Abbreviations

Symbols (in order of appearance)

T	Temperature
Q	Heat distribution
K_c	Thermal conductivity
n	Refractive index
dn/dT	Thermo-optic coefficient
λ_{em}	Emission wavelength
σ_{em}	Emission cross-section
τ	Upper state lifetime
λ_P	Pump wavelength
λ_L	Laser wavelength
P_{out}	Output power
P_{abs}	Absorbed pump power
P_{th}	Threshold pump power
L_i	Internal cavity loss
ν_L	Laser frequency
ν_p	Pump frequency
h	Planck constant
η	Slope efficiency
M^2	Beam quality factor
P_{PE}	Photo-elastic effect
$Q_{bulging}$	Bulging effect
D	Dioptric power of thermal lens
w_p	Pump radius
Δ	Generalized thermo-optic coefficient
η_h	Fractional heat load
M	Thermal lensing sensitivity factor
α	Thermal expansion coefficient
c	Speed of light

Abbreviations

AR	Anti-reflective
BRF	Birefringent filter
CW	Continuous-wave
CW-ML	Continuous-wave mode locking
DM	Dichroic mirror
DPSSL	Diode-pumped solid-state laser
FEA	Finite element analysis
FWHM	Full width at half maximum
HR	Highly reflective
LD	Laser diode
ML	Mode-locked
NA	Numerical aperture
Nd	Neodymium
OC	Output coupler
QD	Quantum defect
QS	Q-switching
RF	Radio frequency
RoC	Radius of curvature
SESAM	Semiconductor saturable absorber mirror
VBG	Volume Bragg gratings

Chapter 1 – Introduction

Lasers have many applications in different areas such as data storage, industrial manufacturing, telecommunication and biomedical fields. The first laser was introduced by Maiman in 1960 [1], and it was based on a ruby crystal with flash lamp pumping. Four years later the first diode-pumped solid-state laser was demonstrated by R.J. Keyes and T.M. Quist [2]. However, the cryogenic cooling was one of the requirements of the diode-pumped solid-state lasers at that time. The great interest in diode-pumped solid-state lasers (DPSSL) is due to the narrow output spectrum of the pumping source in comparison with the other pumping sources such as flash lamps. This narrow output spectrum can improve the efficiency of the laser systems by at least an order of magnitude. In addition to the high efficiency, DPSSL can offer excellent beam quality and high output power which are highly demanded in many applications such as micromachining and nonlinear optics.

Nd:YAG, one of the most famous solid-state lasers and which is still on the market, was diode-pumped for the first time in 1968 [3]. Neodymium-doped Yttrium Orthovanadate (Nd:YVO_4) and Neodymium-doped Gadolinium Orthovanadate (Nd:$GdVO_4$) crystals are among the other well-known host materials. Nd:YVO_4 was first diode-pumped in 1987 [4] and Nd:$GdVO_4$ was first introduced as a laser material in 1992 [5]. Nd:YVO_4 is a common alternative for Nd:YAG and its outstanding features include a large emission cross-section (around five times greater than Nd:YAG), a strong broadband absorption at 808 nm [6] and a polarized laser output. Nd:YVO_4 is now extensively used for pumping of the famous Ti:sapphire lasers and many other lasers with low- to mid- power range (10 W). The main drawback of Nd:YVO_4 is its relatively low thermal conductivity which limits the output power of this crystal. An attractive potential solution to this

issue is to use the crystal of Nd:$GdVO_4$, which has high thermal conductivity [7] and similar laser properties to those of Nd:YVO_4. This research aimed to explore the performance of the Nd:$GdVO_4$ crystal for generation of efficient, high power and high beam quality lasers in both the CW and pulsed regimes.

1.1 Motivation

As mentioned in the previous section, vanadate based Nd-ion doped gain media such as Nd:$GdVO_4$ and Nd:YVO_4 are well-known choices for generation of efficient mid- power (<10 W) high beam quality lasers around 1.06 μm. However, operation at higher powers is still a challenging task mainly due to the thermal lensing effects in these gain media.

During the past decade, the laser diode industry has developed efficient sources for pumping of solid-state lasers at new wavelengths. Thanks to this revolution, it was possible to diode pump the Nd:YVO_4 crystal at a new wavelength of ~ 900 nm instead of the standard pumping at 808 nm and thus to reduce the thermal effects within the gain medium. Extensive research has been made in this area and efficient and high power performance of the Nd:YVO_4 lasers were reported under 914 nm diode pumping [8-14]. However, the maximum achievable output power of Nd:YVO_4 is still limited by its inferior thermal properties. Nd:$GdVO_4$ laser could be a potential alternative to the Nd:YVO_4 on high power operation due to its superior thermal properties and similar spectral features.

Unlike Nd:YVO_4, the high power operation of the Nd:$GdVO_4$ laser crystal under diode pumping of around 914 nm has not been explored yet. The only previous work reported an output power of 3.35 W at 1063 nm in the CW regime [15]. Furthermore, there has been no report on extending this promising pumping approach from the CW to the ML regime.

1.2 Objectives

The overall aim of this research was to explore the performance of Nd:$GdVO_4$ lasers under the 912 nm wavelength pumping in both the CW and pulsed regimes as well as to study the thermal lensing behaviour of such a laser system. More specifically, we were interested to pursue the following goals:

- Investigate the performance of a Nd:$GdVO_4$ laser in the CW regime under the 912 nm pumping to achieve a high power (>10 W) laser with good beam quality;
- Study the thermal lensing behaviour of a Nd:$GdVO_4$ laser under the 912 nm pumping;
- Implement mode-locking technique to study the capabilities of Nd:$GdVO_4$ to generate ultrashort pulses under the 912 nm pumping;
- Investigate discrete wavelength tuning and dual-wavelength operation of a Nd:$GdVO_4$ laser.

1.3 Contributions

The following contributions have been made in this work:

- Characterization of the thermal lensing effect in a 1063 nm Nd:$GdVO_4$ laser under 912 nm pumping. The thermal lensing strength was found to be around two times weaker when compared to the Nd:$GdVO_4$ laser with 808 nm pumping or Nd:YVO_4 laser with 914 nm pumping. The results were published in Applied Physics B journal: M. Nadimi, T. Waritanant, and A. Major, *"Thermal lensing in Nd:$GdVO_4$ laser with direct in-band pumping at 912 nm,"* Appl. Phys. B, 124, 170 (2018) [16]. Chapter 3 of this thesis contains materials from this paper.

- A successful demonstration of high power and high beam quality CW Nd:$GdVO_4$ laser under 912 nm pumping. The results were presented at the Photonics North 2017 conference and were published in Photonics Research journal: M. Nadimi, T. Waritanant, and A. Major, *"High power and beam quality continuous-wave Nd:$GdVO_4$ laser in-band diode-pumped at 912 nm,"* Photonics Res. 5, 346-349 (2017) [17]. Chapter 4 of this thesis contains materials from this paper. Reprinted with permission.
- A successful demonstration of the highest average output power ever obtained for the mode-locked Nd-doped lasers that were pumped around 912 nm. The results were presented at the Photonics North 2017 conference and were published in Laser Physics Letters journal: M. Nadimi, T. Waritanant, and A. Major, *"Passively mode-locked high power Nd:$GdVO_4$ laser with direct in-band pumping at 912 nm,"* Laser Phys. Lett. 15, 15001 (2018) [18]. Chapter 6 of this thesis contains materials from this paper.
- A successful demonstration of an efficient discretely wavelength-tunable Nd:$GdVO_4$ laser operating at four wavelengths of 1063 nm, 1071 nm 1083 nm and 1086 nm using a single birefringent filter in a cavity. The results were presented at the Photonics North 2017 conference and were published in Laser Physics Letters journal: M. Nadimi, T. Waritanant, and A. Major, *"Discrete multi-wavelength tuning of a continuous wave diode-pumped Nd:$GdVO_4$ laser,"* Laser Phys. Lett. 15, 055002 (2018) [19]. Chapter 5 of this thesis contains materials from this paper.

- A successful demonstration of dual-wavelength operation of the Nd:$GdVO_4$ laser with 1063 & 1071 nm, 1063 & 1083 nm and 1083 & 1086 nm wavelength pairs using a single birefringent filter in a cavity. The results were published in Laser Physics journal: M. Nadimi, and A. Major, *"Continuous-wave dual-wavelength operations of a diode-pumped Nd:$GdVO_4$ laser at 1063 & 1071 nm, 1063 & 1083 nm and 1083 &1086 nm,"* Laser Phys. 28, 095001 (2018) [20]. Chapter 5 of this thesis contains materials from this paper.

1.4 Report structure

This report consists of 7 chapters.

Chapter 2 reviews the background of the up to date research. The properties of the Nd:$GdVO_4$ crystal are described and compared with the crystals of Nd:YVO_4 and Nd:YAG. The theory of thermal lensing processes in lasers is discussed and the previous studies of in-band pumping of the Nd:$GdVO_4$ and Nd:YVO_4 crystals around 912 nm are reviewed.

Chapter 3 presents the thermal lensing studies of a Nd:$GdVO_4$ laser under 912 nm pumping. Both experimental data as well as FEA simulation results are provided and discussed. Numerical calculations were also performed to predict the thermal lensing behaviour of a Nd:$GdVO_4$ crystal in different experimental conditions. This chapter is based on [16].

Chapter 4 describes the demonstration of a high power, high beam quality CW Nd:$GdVO_4$ laser under 912 nm pumping. This chapter is based on [17].

Chapter 5 consists of two main parts. Part 1 presents the discrete wavelength tuning operation of a Nd:$GdVO_4$ laser at four wavelengths of 1063 nm, 1071 nm, 1083 nm and 1086 nm.

Part 2 reports on the dual-wavelength operation of a Nd:$GdVO_4$ laser at 1063 & 1071 nm, 1063 & 1083 nm and 1083 & 1086 nm wavelength pairs. This chapter is based on [19, 20].

Chapter 6 consists of two main parts. Part 1 describes the operation principle of the SESAM mode locking technique which is a well-known passive technique for generation of ultrashort laser pulses. Part 2 reports on the first SESAM mode-locked Nd:$GdVO_4$ laser diode-pumped at 912 nm. Second part of this chapter is based on [18].

Chapter 7 presents the conclusion and outlines the possible future work.

References

1. T. H. Maiman, "Stimulated Optical Radiation in Ruby", Nature **187**, 493–494 (1960).
2. R. J. Keyes and T. M. Quist, "Injection Luminescent Pumping of $CaF_2:U^{3+}$ with GaAs Diode Lasers," Appl. Phys. Lett. **4,** 50–52 (1964).
3. M. Ross, "YAG laser operation by semiconductor laser pumping," Proc. IEEE **56**, 196–197 (1968).
4. R. A. Fields, M. Birnbaum, and C. L. Fincher, "Highly efficient Nd:YVO_4 diode-laser end-pumped laser," Appl. Phys. Lett. **51,** 1885–1886 (1987).
5. A. I. Zagumennyĭ, V. G. Ostroumov, I. A. Shcherbakov, T. Jensen, J. P. Meyen, and G. Huber, "The Nd:GdVO 4 crystal: a new material for diode-pumped lasers," Sov. J. Quantum Electron. **22**, 1071–1072 (1992).
6. W. Koechner, Solid-State Laser Engineering, (Springer, 2006).
7. P. A. Studenikin, A. I. Zagumennyi, Y. D. Zavartsev, P. A. Popov, and I. A. Shcherbakov, "$GdVO_4$ as a new medium for solid-state lasers: some optical and thermal properties of crystals doped with Cd^{3+}, Tm^{3+}, and Er^{3+} ions," Quantum Electron. **25**, 1162–1165 (1995).

8. D. Sangla, M. Castaing, F. Balembois, and P. Georges, “Highly efficient Nd:YVO_4 laser by direct in-band diode pumping at 914 nm,” Opt. Lett. **34**, 2159–2161 (2009).
9. X. Délen, F. Balembois, O. Musset, and P. Georges, “Characteristics of laser operation at 1064 nm in Nd:YVO_4 under diode pumping at 808 and 914 nm,” J. Opt. Soc. Am. B **28**, 52–57 (2011).
10. T. Waritanant and A. Major, “Thermal lensing in Nd:YVO_4 laser with in-band pumping at 914 nm,” Appl. Phys. B **122**, 135 (2016).
11. T. Waritanant and A. Major, “Diode-pumped Nd:YVO_4 laser with discrete multi-wavelength tunability and high efficiency,” Opt. Lett. **42**, 1149–1152 (2017).
12. L. Chang, C. Yang, X. J. Yi, Q. K. Ai, L. Y. Chen, M. Chen, G. Li, J. H. Yang, and Y. F. Ma, “914 nm LD end-pumped 31.8 W high beam quality E-O Q-switched Nd:YVO_4 laser without intracavity polarizer,” Laser Phys. **22**, 1369–1372 (2012).
13. T. Waritanant and A. Major, "Discretely selectable multiwavelength operation of a semiconductor saturable absorber mirror mode-locked Nd:YVO_4 laser," Opt. Lett. **42**, 3331–3334 (2017).
14. T. Waritanant and A. Major, “High efficiency passively mode-locked Nd:YVO_4 laser with direct in-band pumping at 914 nm,” Opt. Express **24**, 12851–12855 (2016).
15. J. L. Ma, B. Xiong, L. Guo, P. F. Zhao, L. Zhang, X. C. Lin, J. M. Li, and Q. D. Duanmu, “Low heat and high efficiency Nd:$GdVO_4$ laser pumped by 913 nm,” Laser Phys. Lett. **7**, 579–582 (2010).
16. M. Nadimi, T. Waritanant, and A. Major, “Thermal lensing in Nd:$GdVO_4$ laser with direct in-band pumping at 912 nm,” Appl. Phys. B, **124**, 170 (2018).
17. M. Nadimi, T. Waritanant, and A. Major, “High power and beam quality continuous-wave

Nd:$GdVO_4$ laser in-band diode-pumped at 912 nm," Photonics Res. **5**, 346–349 (2017).

18. M. Nadimi, T. Waritanant, and A. Major, "Passively mode-locked high power Nd:$GdVO_4$ laser with direct in-band pumping at 912 nm," Laser Phys. Lett. **15**, 15001 (2018).
19. M. Nadimi, T. Waritanant, and A. Major, "Discrete multi-wavelength tuning of a continuous wave diode-pumped Nd:$GdVO_4$ laser," Laser Phys. Lett. **15**, 055002 (2018).
20. M. Nadimi, and A. Major, "Continuous-wave dual-wavelength operations of a diode-pumped Nd:$GdVO_4$ laser at 1063 & 1071 nm, 1063 & 1083 nm and 1083 &1086 nm," Laser Phys. **28**, 095001 (2018).

Chapter 2 – Background

This chapter reviews the background of the relevant research. The theory of thermal lensing effect in lasers is discussed and the previous reports of Nd:$GdVO_4$ and Nd:YVO_4 lasers under ~ 912 nm diode pumping are reviewed.

2.1 Thermal lensing

The output power of the diode-pumped solid-state laser systems is usually limited by the thermal lensing effect. Thermal lensing affects the stability of a resonator and degrades the output beam quality. In extreme cases, a large thermal gradient can result in mechanical failure of the crystal. The following section describes the theory of the thermal lensing process in solid-state lasers.

2.1.1 Thermal lensing theory

Solid-state laser systems dissipate a certain amount of heat during their operation. The heat arises due to different reasons, but mainly due to the energy difference between the pump level and the higher laser level as well as the energy difference between the lower laser level and the ground state [1]. The described energy difference between the pump photon and the photon of the produced laser output is known as quantum defect (QD) and is given as

$$QD = h\nu_{Pump} - h\nu_{Laser} . \quad (2\text{-}1)$$

QD also can be described based on the percentage of the pump photon energy that is converted to heat using equation 2-2:

$$QD' = \left(1 - \frac{\lambda_{Pump}}{\lambda_{Laser}}\right) \times 100\% . \quad (2\text{-}2)$$

The produced heat in the crystal must be directed to the edges of the crystal to be removed. This ultimately results in a non-uniform temperature distribution in the gain medium which can be described by the heat diffusion equation:

$$\nabla^2 T(x,y,z) = -\frac{Q(x,y,z)}{k_c} \quad , \qquad (2\text{-}3)$$

where T is the temperature profile, Q is the heat distribution and k_c is the thermal conductivity of the material. For the case of a rod-shaped crystal, equation 2-3 can be solved analytically. However, FEA method should be used to get the temperature profiles of the laser crystal in case of more complicated geometries.

The temperature gradient inside the crystal causes changes in the refractive index (n) of the crystal through different effects. One of the most important ones is the change in the refractive index due to the thermo-optic effect. This effect is quantified by the gain medium thermo-optic coefficient (d*n*/d*T*). Additional refractive index changes can be introduced by the thermally induced mechanical stress (photo-elastic effect). In general, the change of the refractive index of the crystal due to the thermo-optic effect and thermal stresses can be described by

$$\mathrm{n(x,y,z)} = n_0(\mathrm{x,y,z}) + \Delta n_T\,(\mathrm{x,y,z}) + \Delta n_\varepsilon(\mathrm{x,y,z}), \qquad (2\text{-}4)$$

where n_0 is the initial refractive index, n_T and n_ε are thermally induced and stress induced changes of refractive index, respectively. Furthermore, the thermally induced mechanical stress can result in bulging of the crystal surfaces. The induced changes in the refractive index together with the deformation of the crystal cause a distortion of the optical beam within the gain medium. Usually, these behaviors are modeled into the system by considering a virtual thin lens inside the crystal.

Therefore, this effect is called "thermal lensing". The focal length (or dioptric power[1]) of the thermal lens describes the strength of the thermal lensing effect.

There are various experimental techniques to calculate the thermal lensing effect. In the present work, the beam width measurement technique in combination with ABCD matrix analysis has been used to model the thermal lensing effect. Furthermore, FEA was also used to validate the experimental data.

2.1.2 Laser cavity design with thermal lensing

One of the most important criteria in designing a laser cavity is to choose the lens/mirror system and distances between each element such that a good overlap between the pump beam and the oscillating laser beam will be obtained (this is called mode matching). The laser cavity can be designed and simulated using an ABCD matrix analysis, where optical elements are described using a 2×2 matrix. In the present work, we mainly used the **reZonator** software [2] and the **LASCAD** software [3] for the simulation of the laser cavity and beam size analysis.

The transfer matrices of simple optical components are given by:

Flat Mirror $=\begin{bmatrix}1 & 0\\ 0 & 1\end{bmatrix}$, Curved mirror $=\begin{bmatrix}1 & 0\\ -2/R & 1\end{bmatrix}$, Free space propagation $=\begin{bmatrix}1 & L\\ 0 & 1\end{bmatrix}$, crystal $=\begin{bmatrix}1 & d/n\\ 0 & 1\end{bmatrix}$

where L is the propagation distance, R is the radius of curvature, d is the crystal length and n is the refractive index.

The stability of the system as well as the spot size in the cavity can be monitored by changing the distances between each element. The main goal of the cavity design is to obtain a

[1] Dioptric power is equal to the inverse of focal length taken in meters

good overlap between the laser beam size and the pump beam size within the crystal. In this work, effective thermal lens was considered as a thin lens at the center of the gain medium.

As an example, an equivalent laser cavity of a four mirror cavity is demonstrated in Fig. 2-1-a. The corresponding beam profile which was obtained by the **reZonator software** is shown in Fig. 2-1-b. In Fig. 2-1, M1 is a plane mirror, L1, L2, L3 and L4 are the propagation distances in air, Cr1 and Cr2 are the first and second halves of the same laser crystal, F1 is the effective thermal lens (the focal length considered to be 300 mm) and M2 and M3 are lenses equivalent to the concave mirrors used in the experiment (radii of curvatures are 400 and 500 mm, respectively), and M4 is a flat output coupler. Fig. 2-1-b demonstrates a reasonable mode matching between the laser beam size and the pump spot size (275 µm) within the crystal.

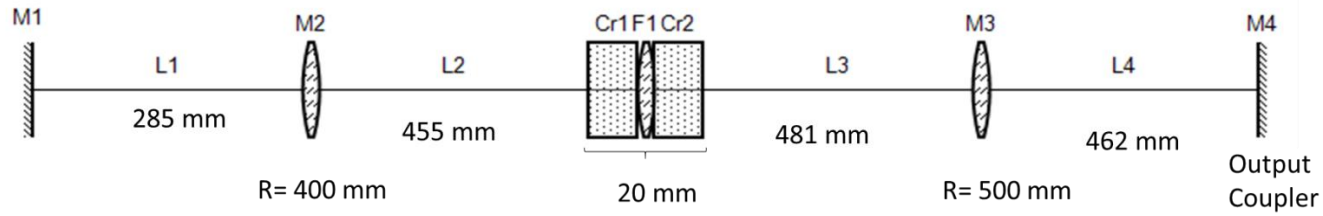

(a)

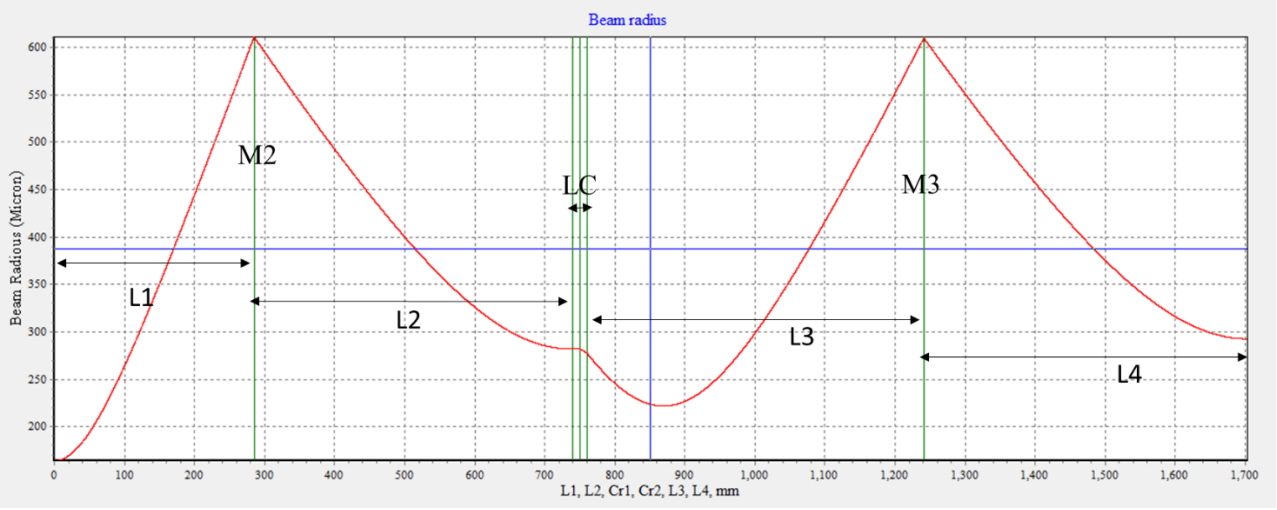

(b)

Fig. 2-1. Laser cavity. (a) Schematic diagram of the laser cavity used in ABCD matrix calculation; (b) beam radius evolution inside the designed resonator.

2.2 Crystal properties

2.2.1 Host and dopant materials

Laser gain media usually consist of a host material and dopants. Generally, dopants belong to the rare-earth metal ions (e.g. Nd, Ho, Er, Yb) or transition-metal ions (e.g. Cr, Ti, Co, Ni). Typically, the host material keeps the dopant in place and determines the material properties such as thermal conductivity and refractive index while the dopants determine the emission and absorption spectral properties of the gain medium. Neodymium (Nd) doped crystals are the most popular gain media for solid-state lasers. The following section discusses the properties of neodymium-doped crystals.

2.2.2 Neodymium-doped crystals ($Nd:GdVO_4$ and $Nd:YVO_4$)

As briefly described in chapter 1, Nd:YAG, $Nd:YVO_4$ and $Nd:GdVO_4$ crystals are all well-known laser materials used in solid-state lasers. Among the Nd-doped crystals, Nd:YAG is a traditional choice for generation of 1.06 μm lasers. However, $Nd:YVO_4$ is one of the common alternatives to Nd:YAG as it can offer much higher emission cross-section, stronger broadband absorption at 808 nm and inherent birefringence. On the other hand, relatively low thermal conductivity of $Nd:YVO_4$ is its main disadvantage which plays an important role in limiting the output power of this crystal. $Nd:GdVO_4$ is more appropriate for high power applications than $Nd:YVO_4$. The reason is that the thermal conductivity of $Nd:GdVO_4$ is almost twice as high as that of the $Nd:YVO_4$ while their spectral properties are very similar. This property makes the $Nd:GdVO_4$ laser to be known as a promising alternative to $Nd:YVO_4$ DPSSLs. Table 2-1 provides the comparison of the optical and thermal properties of these three Nd-doped crystals.

Table 2-1. Properties of Nd:YVO_4, Nd:$GdVO_4$, and Nd:YAG crystals

Laser Crystal	λ_{em} (nm)	σ_{em} (10^{-19} cm^2) @ 1064 nm	$\Delta\lambda$ (nm)	k_c ($Wm^{-1}K^{-1}$)	τ (µs)	n
Nd:YVO_4	1064	14.1 [4]	1.1 [4]	5.1 [5]	84.4 [4]	no = 1.9573 ne = 2.1652 [6]
Nd:$GdVO_4$	1063	10.3 [4]	1 [4]	11.7 [7]	83.4 [4]	no = 1.9854 ne = 2.1981 [7]
Nd:YAG	1064	2.8 [1]	0.6 [8]	14 [1]	230 [1]	1.82 [8]

λ_{em}: emission wavelength, σ_{em}: emission cross-section at emission wavelength, $\Delta\lambda$: gain bandwidth, n: refractive index, ordinary or extraordinary, τ: upper state lifetime (1% Nd doping) and k_c: thermal conductivity (there is still a debate on the true values of thermal conductivities of Nd:YVO_4 and Nd:$GdVO_4$ [1, 9-12]).

2.2.2.1 Nd:$GdVO_4$ and Nd:YVO_4

Both $GdVO_4$ and YVO_4 crystals have a tetragonal structure, and they are uni-axial crystals. Nd^{3+} ions replace Gd^{3+} and Y^{3+} ions in the $GdVO_4$ and YVO_4 crystals, respectively. Lattice parameters of $GdVO_4$ and YVO_4 are a=b=0.721 nm, c=0.635 nm [7] and a=b=0.712 nm, c=0.629 nm [13], respectively. Usually, $GdVO_4$ and YVO_4 crystals cut along the a-axis are preferred because of the better absorption/emission characteristics of the light polarized along the c-axis (also known as π-polarization). The absorption spectra of the Nd:$GdVO_4$ and Nd:YVO_4 crystals for both π (E//c) and σ (E//a) polarizations are shown in Fig. 2-2 and Fig. 2-3, respectively. Fig. 2-4 illustrates the stimulated emission cross-section of vanadate crystals. Considering data in table 2-1 and Fig. 2-4, the στ product (which is inversely proportional to the threshold pump power) of Nd:$GdVO_4$ would be smaller than that of Nd:YVO_4, but greater than that of Nd:YAG. Therefore, this won't be a significant drawback for a Nd:$GdVO_4$ laser oscillation [4].

The geometry of the Nd:$GdVO_4$ crystal used in the study is demonstrated in Fig. 2-5.

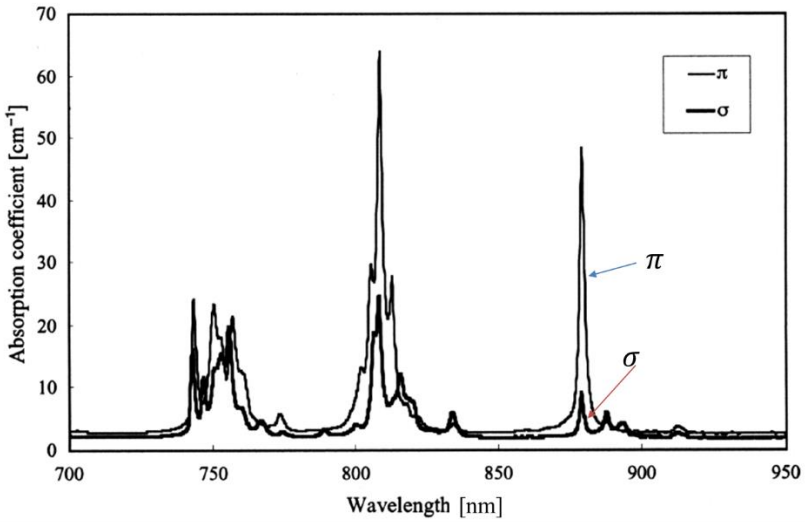

Fig. 2-2. Absorption spectra of 2-at.% Nd-doped Nd:$GdVO_4$ [14]. © 2003 OSA, reprinted with permission.

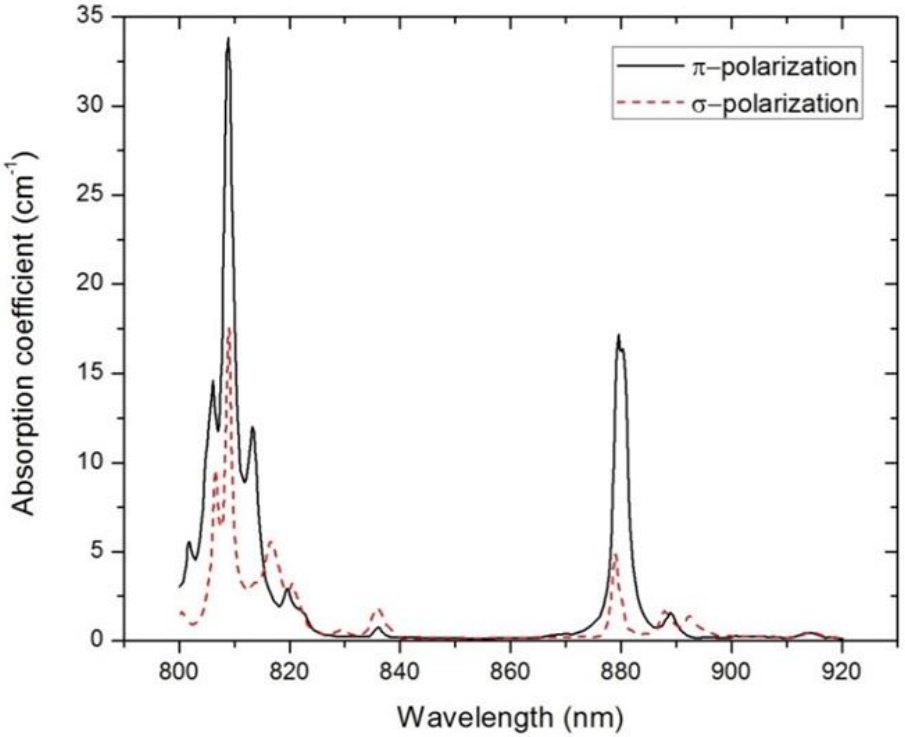

Fig. 2-3. Absorption spectra of 1-at.% Nd-doped Nd:YVO_4 [15].

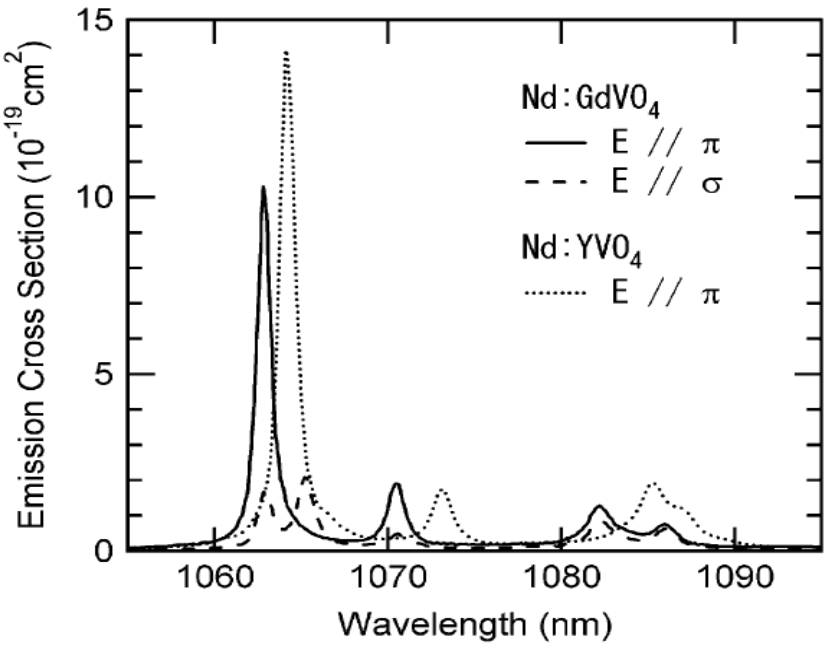

Fig. 2-4. Stimulated emission cross-sections of 1-at.% Nd-doped Nd:$GdVO_4$ and Nd:YVO_4 [4]. © 2005 IEEE.

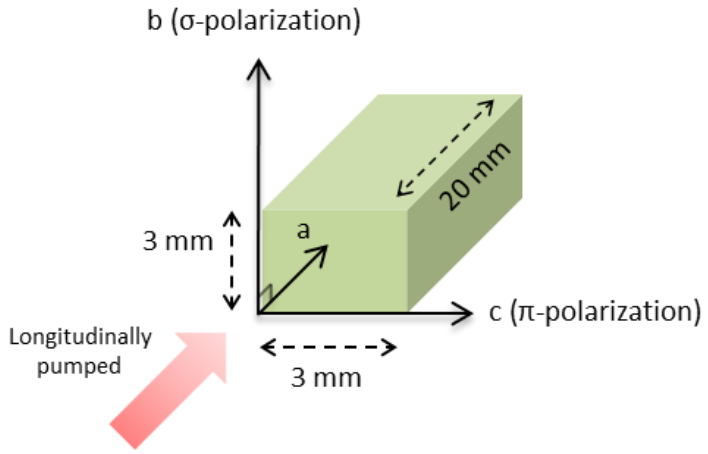

Fig. 2-5. The geometry of the crystal used in the study.

The energy level diagram of the Nd:$GdVO_4$ and Nd:YVO_4 and the corresponding electron transitions are shown in Fig. 2-6. The conventional pump and laser wavelengths are 808 nm and 1063/1064 nm, respectively. As discussed in Chapter 1, instead of traditional 808 nm pumping, a novel ~ 912/914 nm pumping was proposed to decrease the thermal problems in Nd:$GdVO_4$ and Nd:YVO_4 lasers [16-26].

As demonstrated in Fig. 2-6, the energy difference between the pump and laser photons (λ=1063/1064 nm) is much lower in case of 912/914 nm pumping than with 808 nm pumping. This lower energy difference reduces the fractional heat load (a fraction of the absorbed pump power that is dissipated as heat in a gain medium which can be approximated by quantum defect ratio as $1–\lambda_P/\lambda_L$, where λ_P and λ_L are the pump and laser wavelengths) from 24.1% to 14.2%. Another interesting point about the Nd:$GdVO_4$ and Nd:YVO_4 crystals is that the 912/914 nm wavelength can also be produced by these crystals. In some experiments [22, 23], two vanadate crystals were used in the laser system, one for generating at 912/914 nm (i.e. as a pump source) and the other for the generation of the laser output at 1342 nm.

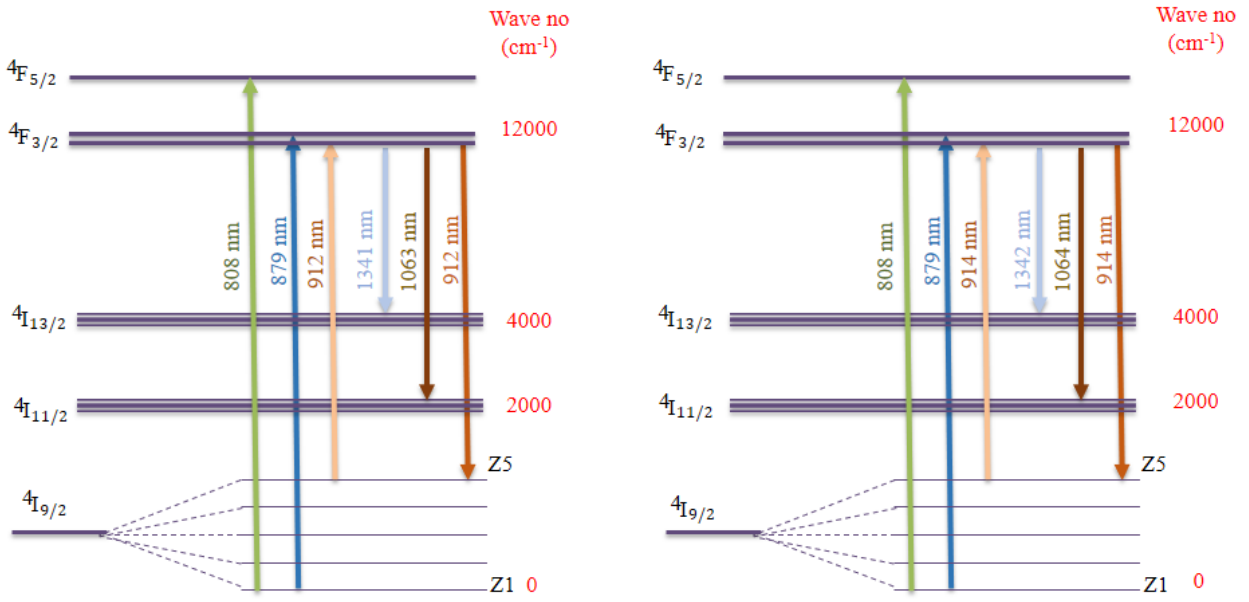

Fig. 2-6. Energy level diagrams of Nd:$GdVO_4$ crystal transitions on the left [24] and Nd:YVO_4 crystal on the right.

Pumping of the vanadate lasers around 912/914 nm can also maximize the slope efficiency of a laser system. In order to investigate the effect of pump wavelengths on the slope efficiency, the output power of a CW laser should be analyzed. The output power of a laser in the CW regime beyond the threshold power can be modeled using equation 2-5:

$$P_{out} = \frac{-\ln(1-T)}{-\ln(1-T)+L_i} \times \frac{v_L}{v_P} \times (P_{abs} - P_{th}), \quad (2\text{-}5)$$

where P_{out}, P_{abs} and P_{th} are the output power, absorbed pump power and threshold power, respectively. T is the transmission of the output coupler and L_i is the internal cavity loss. v_L stands for the laser frequency and v_p corresponds to the pump frequency.

Equation 2-5 can also be presented based on the pump wavelength λ_P and laser wavelength λ_L instead of the corresponding frequencies as:

$$P_{out} = \frac{-\ln(1-T)}{-\ln(1-T)+L_i} \times \frac{\lambda_P}{\lambda_L} \times (P_{abs} - P_{th}). \quad (2\text{-}6)$$

Assuming a perfect mode matching between the pump and laser modes, the threshold pump power of a 4-level laser can be expressed by [27, 28]:

$$P_{th} = \frac{\pi h v_P w^2 (Li - \ln(1-T))}{2\sigma\tau} \quad , \quad (2\text{-}7)$$

where h is Planck's constant, w is the pump beam waist, τ is the fluorescence lifetime and σ is the emission cross-section.

Using equation 2-6, the slope efficiency (η) of a CW laser system can be expressed as [29]:

$$\eta = \frac{-\ln(1-T)}{-\ln(1-T)+L_i} \times \frac{\lambda_P}{\lambda_L}. \quad (2\text{-}8)$$

Based on equation 2-8, one can deduce that pumping the vanadate lasers around 912/914 nm instead of 808 nm can maximize the slope efficiency of the laser system.

Despite the promising results of the longer wavelengths pumping approach, very little research was conducted into pumping of the Nd:$GdVO_4$ lasers at 912 nm [21-26]. The next section reviews the history of Nd:YVO_4 and Nd:$GdVO_4$ lasers with in-band pumping around 912/914 nm.

2.3 Previous records of Nd:YVO_4 laser in-band pumped at 914 nm

In 2009, D. Sangla et al. presented the first 1064 nm Nd:YVO_4 laser that was diode-pumped at 914 nm [25]. The gain medium was a 10-mm-long 1.5 at. % Nd-doped Nd:YVO_4 crystal. The cavity consisted of three mirrors (Fig. 2-7): one mirror deposited on the crystal surface, a concave mirror and a plane output coupler (15% OC). At the maximum laser diode (LD) pump power of 35 W, 14.6 W was absorbed and the highest laser output power of 11.5 W was reported. The optical efficiency and slope efficiency were found to be as high as 78.7% and 80.7%, respectively.

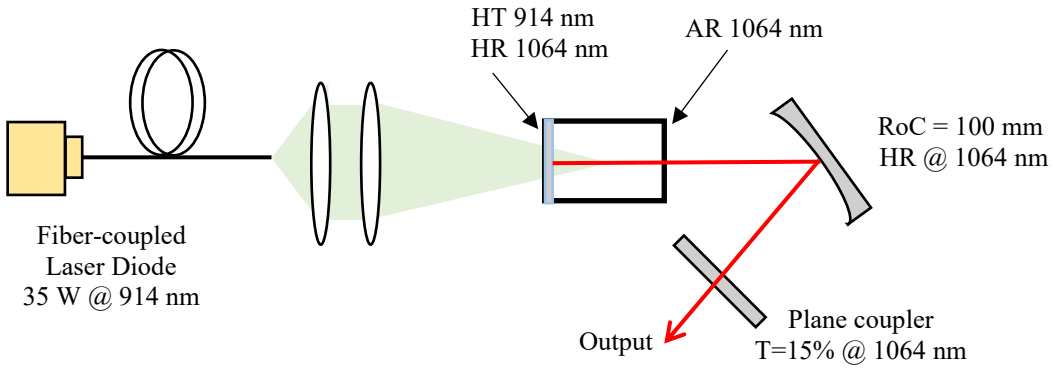

Fig. 2-7. Schematic layout of the experimental setup of Nd:YVO_4 laser [25]. HT: highly transmissive, HR: highly reflective, AR: anti-reflective and RoC: radius of curvature.

In 2011, a comparative study between the 808 nm and 914 nm pumping of Nd:YVO_4 crystals for laser operation at 1064 nm was reported by X. Delen et al. [21]. Considering very different absorption spectra at 808 nm and 914 nm (Fig. 2-2), the authors used two Nd:YVO_4 crystals with different doping concentrations in their experiment (1.5% doped crystal for 914 nm pumping and 0.1% for 808 nm pumping). The comparison between the two pumping configurations was carried out at the same absorbed pump power level. Using a similar setup, operation in the CW regime resulted in slope efficiencies of 81% and 58% for 914 nm pumping and 808 nm pumping, respectively. This significant difference was mainly due to the lower quantum defect of the 914 nm pumping scheme and clearly demonstrated one of its benefits.

In addition, in 2011 X. Ding et al. reported the first 1342 nm Nd:YVO_4 laser in-band pumped at 914 nm [22]. To ensure good beam quality of a pump source, a 914 nm Nd:YVO_4 laser was used to excite the 1342 nm laser instead of a 914 nm laser diode. In order to study the influence of doping concentration on laser performance, a 1.0- at.% doped Nd:YVO_4 crystal (8 mm-long) and a 3.0- at.% doped Nd:YVO_4 crystal (4 mm-long) were used in the experiment. The maximum output power of 0.86 W at 1342 nm was achieved for 1.0- at.% doped Nd:YVO_4 crystal under 1.82 W of absorbed pump power, corresponding to a slope efficiency of 65.4%. Higher doping concentration resulted in the reduction of the slope efficiency which was attributed to the shorter upper laser level lifetime.

Very recently, T. Waritanant et al. performed comprehensive studies on the performance of Nd:YVO_4 laser under 914 nm diode pumping. In the study of the thermal lensing effect in a 0.5 at.% doped 12 mm-long Nd:YVO_4 crystal, the thermal lensing strength was measured using a 3 mirror cavity [26]. The authors showed that the strength of thermal lensing with 914 nm pumping was more than two times weaker than that with traditional 808 nm. Later they examined mode-locked operation of a 1.5 at.% doped 20 mm-long Nd:YVO_4 crystal using a SESAM as one of the end mirrors of a 5 mirror cavity. The authors achieved 6.7 W of average output power with pulse duration of 16 ps. The reported slope efficiency was 77.1% which was the highest slope efficiency for the ML Nd-doped lasers [29].

Furthermore, discrete wavelength operation of a diode-pumped Nd:YVO_4 laser at three different wavelengths was demonstrated using a single birefringent filter plate in a three mirror cavity [30]. The laser achieved maximum output powers of 4.78 W, 3.89 W and 3.92 W at 1064 nm, 1073 nm and 1085 nm, respectively. The mode-locked operation of these lasers has also been reported [31]. The authors also were able to demonstrate CW dual-wavelength operations for a

diode-pumped Nd:YVO_4 laser at (1064, 1073) and (1073, 1085) nm by using a two-plate birefringent filter in a three mirror cavity [32].

2.4 Previous records of Nd:$GdVO_4$ laser in-band pumped at 912 nm

The first 1063 nm Nd:$GdVO_4$ laser that was diode-pumped around 912 nm was demonstrated by J.L. Ma, et al. in 2010 [24]. The gain medium was a 1.1 at.% Nd-doped Nd:$GdVO_4$ crystal with the dimensions of 3×2×20 mm^3. The authors designed a plano-concave resonator (Fig. 2-8) to achieve the highest overlap between the pumping beam (diameter of 380 μm) and oscillating laser beam. The cavity consisted of a dichroic mirror with anti-reflection coating at 913 nm and high-reflection coating at 1064 nm and a concave mirror as the output coupler (20% OC). The laser threshold was observed at the absorbed pump power of 0.21 W. At the maximum laser diode pump power of 8.0 W, 4.30 W was absorbed and the highest laser output power of 3.35 W was reported. The optical efficiency was reported to be 77.2 % and the slope efficiency was found to be 81.2%, which was very close to the theoretical limitation imposed by the quantum defect at 85.9%.

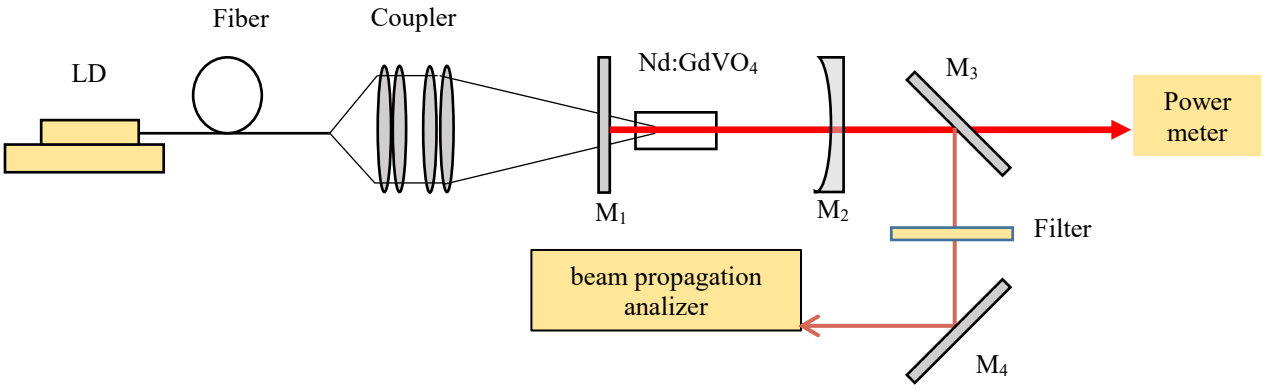

Fig. 2-8. Schematic layout of the experimental setup of Nd:$GdVO_4$ laser [24]. LD: laser diode, M_1: flat dichroic mirror, M_2: concave mirror (OC), M_3 and M_4: flat mirrors. The filter is coated for HR at 913 and AR at 1063 nm.

The first 1341 nm Nd:$GdVO_4$ laser with 912 nm direct pumping was reported by Y. L. Li et al. in 2012 [23]. The authors used two Nd:$GdVO_4$ crystals in their laser system, the first one as the pumping source to generate a 912 nm pumping beam and the second one as a gain medium to generate radiation at 1341 nm. The main pump source included a 808 nm fiber-coupled laser diode and a Nd:$GdVO_4$ crystal; The output beam of a laser diode was focused into a 0.2 at % doped a-cut 3×3×5 mm^3 Nd:$GdVO_4$ crystal and created the 912 nm pumping beam. A concave mirror with 5% transmittance was used as an output coupler. Furthermore, a focusing lens was used after the output coupler to provide a better mode matching between the pump and oscillating beams in the second Nd:$GdVO_4$ crystal (1.0 at % doped 3×3×8 mm^3). The authors designed a simple two-mirror plano-concave resonator for the second Nd:$GdVO_4$ crystal to generate the 1341 nm laser. The maximum CW output power of 542 mW at 1341 nm was achieved with 5 % OC under 1.14 W of the absorbed pump power. The slope efficiency was reported to be 56.6%.

Table 2-2 summarizes the performance of Nd:$GdVO_4$ and Nd:YVO_4 lasers under 912/914 nm pumping. As can be seen, so far there has been no report on Nd:$GdVO_4$ laser with high output power.

Table 2-2. Summary of the performance of Nd:$GdVO_4$ and Nd:YVO_4 lasers under 912 nm or 914 nm pumping.

Author	Laser	Output power (W)	Opt-to-opt efficiency (%)	Slope efficiency (%)	year
D. Sangla et al [25]	Nd:YVO_4 CW 1064 nm	11.5	78.7	80.7	2009
X. Delen et al [21]	Nd:YVO_4 CW 1064 nm	~ 11.7	~ 79	81	2011
Waritanant et al [29]	Nd:YVO_4 ML 1064 nm	6.7	60.7	77.1	2016
Waritanant et al [30]	Nd:YVO_4 1064 1073 1085	 4.78 3.89 3.92	 43.3 35.2 35.5	 49.8 46.5 45.7	2017
X. Ding et al [22]	Nd:YVO_4 CW 1342 nm	0.860	47.25	65.4	2011
J.L. Ma et al [24]	Nd:$GdVO_4$ CW 1064 nm	3.35	77.2	81.2	2010
Y. L. Li et al [23]	Nd:$GdVO_4$ CW 1341 nm	0.542	47.5	56.6	2012

References

1. W. Koechner, *Solid-State Laser Engineering*, (Springer, 2006).
2. "Rezonator software." [Online]. Available: www.rezonator.orion-project.org.
3. "LAS-CAD Software." [Online]. Available: www.las-cad.com
4. Y. Sato and T. Taira, "Comparative study on the spectroscopic properties of Nd:$GdVO_4$ and Nd:YVO_4 with hybrid process," *IEEE J. Sel. Top. Quantum Electron.*, **11**, 613–620 (2005).
5. X. Huai and Z. Li, "Thermal stress analysis of a Nd:YVO_4 laser medium end pumped by a Gaussian beam," *Appl. Phys. Lett.*, **92**, 41121 (2008).
6. "foctek.net." [Online]. Available: www.foctek.net/products/Nd_YVO4.htm.
7. "foctek.net." [Online]. Available: www.foctek.net/products/Nd_GdVO4.htm.

8. "foctek.net." [Online]. Available: www.foctek.net/products/Nd_YAG.htm.

9. J. Didierjean, E. Herault, F. Balembois, and P. Georges, "Thermal conductivity measurements of laser crystals by infrared thermography. Application to Nd:doped crystals," Opt. Express **16**, 8995–9010 (2008).

10. J. Morikawa, C. Leong, T. Hashimoto, T. Ogawa, Y. Urata, S. Wada, M. Higuchi, and J. Takahashi, "Thermal conductivity/diffusivity of Nd^{3+} doped $GdVO_4$, YVO_4, $LuVO_4$, and $Y_3Al_5O_{12}$ by temperature wave analysis," J. Appl. Phys. **103**, 63522 (2008).

11. Y. Sato and T. Taira, "The studies of thermal conductivity in $GdVO_4$, YVO_4, and $Y_3Al_5O_{12}$ measured by quasi-one-dimensional flash method," Opt. Express **14**, 10528–10536 (2006).

12. R. Paschotta, "Encyclopedia of laser physics and technology." [Online]. Available: www.rp-photonics.com/vanadate_lasers.html.

13. H. H. Yu, H. J. Zhang, and J. Y. Wang, "Growth and Characterization of Vanadate Laser Crystals," *Acta Phys. Pol. A* **124**, 301–304 (2013).

14. T. Ogawa, Y. Urata, S. Wada, K. Onodera, H. Machida, H. Sagae, M. Higuchi and K. Kodaira, "Efficient laser performance of Nd:$GdVO_4$ crystals grown by the floating zone method," *Opt. Lett.* **28**, 2333-2335 (2003).

15. L. McDonagh, R. Wallenstein, R. Knappe, and A. Nebel, "High-efficiency 60 W TEM_{00} Nd:YVO_4 oscillator pumped at 888 nm," *Opt. Lett.* **31**, 3297-3299 (2006).

16. H. J. Zhang, L. Zhu, X. L. Meng, Z. H. Yang, C. Q. Wang, W. T. Yu, Y. T. Chow, and M. K. Lu, "Thermal and Laser Properties of Nd:YVO_4 Crystal," Cryst. Res. Technol. **34**, 1011–1016 (1999).

17. N. Pavel, T. Dascalu, G. Salamu, O. Sandu, A. Leca, and V. Lupei, "Q-switched Nd lasers pumped directly into the $^4F_{3/2}$ emitting level," Opt. Commun. **282**, 4749–4754 (2009).

18. V. Lupei, N. Pavel, Y. Sato, and T. Taira, "Highly efficient 1063-nm continuous-wave laser emission in Nd:$GdVO_4$," Opt. Lett. **28**, 2366–2368 (2003).

19. Y.-F. Lü, J. Xia, J.-G. Wang, G.-C. Sun, X.-H. Zhang, A.-F. Zhang, X.-D. Yin, L. Bao, and H. Quan, "High-efficiency Nd:$GdVO_4$ laser at 1341 nm under 880 nm diode laser pumping into the emitting level," Opt. Commun. **282**, 3565–3567 (2009).

20. J. Gao, X. Yu, X. D. Li, F. Chen, K. Zhang, R. P. Yan, J. H. Yu, and Y. Z. Wang, "456-nm deep-blue laser generation by intracavity frequency doubling of Nd:$GdVO_4$ under 879-nm diode pumping," Laser Phys. **19**, 111–114 (2009).

21. X. Délen, F. Balembois, O. Musset, and P. Georges, "Characteristics of laser operation at 1064 nm in Nd:YVO_4 under diode pumping at 808 and 914 nm," J. Opt. Soc. Am. B **28**, 52–57 (2011).

22. X. Ding, S.-J. Yin, C.-P. Shi, X. Li, B. Li, Q. Sheng, X.-Y. Yu, W.-Q. Wen, and J.-Q. Yao, "High efficiency 1342 nm Nd:YVO_4 laser in-band pumped at 914 nm," Opt. Express **19**, 14315–14320 (2011).

23. Y. L. Li, J. Y. Liu, and Y. C. Zhang, "High efficiency 1341 nm Nd:$GdVO_4$ laser in-band pumped at 912 nm," Laser Phys. **22**, 547–549 (2012).

24. J. L. Ma, B. Xiong, L. Guo, P. F. Zhao, L. Zhang, X. C. Lin, J. M. Li, and Q. D. Duanmu, "Low heat and high efficiency Nd:$GdVO_4$ laser pumped by 913 nm," Laser Phys. Lett. **7**, 579–582 (2010).

25. D. Sangla, M. Castaing, F. Balembois, and P. Georges, "Highly efficient Nd:YVO_4 laser by direct in-band diode pumping at 914 nm," Opt. Lett. **34**, 2159–2161 (2009).

26. T. Waritanant and A. Major, "Thermal lensing in Nd:YVO_4 laser with in-band pumping at 914 nm," Appl. Phys. B **122**, 135 (2016).

27. W. P. Risk, “Modeling of longitudinally pumped solid-state lasers exhibiting reabsorption losses,” *J. Opt. Soc. Am. B* **5**, 1412-1423 (1988).
28. E. Alimohammadian and A. Major, “Modeling of a CW Nd:YVO_4 laser longitudinally pumped by high power VCSEL modules at 808 nm,” in *SPIE LASE*, 89591D (2014).
29. T. Waritanant and A. Major, “High efficiency passively mode-locked Nd:YVO_4 laser with direct in-band pumping at 914 nm,” Opt. Express **24**, 12851–12855 (2016).
30. T. Waritanant and A. Major, “Diode-pumped Nd:YVO_4 laser with discrete multi-wavelength tunability and high efficiency,” Opt. Lett. **42**, 1149–1152 (2017).
31. T. Waritanant and A. Major, “Discretely selectable multi-wavelength operation of a SESAM mode-locked Nd:YVO_4 laser,” Optics Letters. **42**, 3331-3334 (2017).
32. T. Waritanant and A. Major, “Dual-Wavelength CW Operations at 1064.1 & 1073.1 nm and 1064.1 & 1085.3 nm of Nd:YVO_4 Laser,” Appl. Phys. B **124**, 87 (2018).

Chapter 3 – Thermal lensing in Nd:$GdVO_4$ laser with direct in-band pumping at 912 nm[1]

The generation of high power laser radiation with high beam quality and high efficiency needs a proper laser cavity design. As discussed in chapter 2, one of the key components in the design procedure is the true estimation of the thermal lensing strength inside the crystal. The focal length of the thermal lens has a significant effect on the mode matching between the pump and laser beams, and it also affects the stability of the entire system. This chapter presents the thermal lensing studies of a Nd:$GdVO_4$ laser under 912 nm pumping.

3.1 Introduction

As discussed in chapter 2, strong thermal lensing degrades the laser beam quality and reduces the stability of a laser cavity. Fracture of the laser crystal could be another consequence of strong thermal lensing effects at high output powers [1]. Notable work has been done to reduce the thermal lensing problems in solid-state lasers and some methods proposed were composite crystals [2] and double end pumping [3]. However, the most efficient method was based on pumping of the Nd:YVO_4 and Nd:$GdVO_4$ crystals around 912 nm (i.e. close to the 1064 nm emission line) [4-16].

There have been a few reports in which the performance of Nd:YVO_4 and Nd:$GdVO_4$ lasers has been characterized with the 912-914 nm pumping [4, 5, 7, 10, 12, 14-16]. However, there has been no report on detailed thermal lensing analysis of Nd:$GdVO_4$ lasers with such a

[1] This chapter contains material from [M. Nadimi, T. Waritanant, and A. Major, *"Thermal lensing in Nd:$GdVO_4$ laser with direct in-band pumping at 912 nm,"* Appl. Phys. B, **124**, 170 (2018)]. Reprinted by permission. © 2018 Springer. All rights reserved.

pumping scheme. Taking into account that Nd:$GdVO_4$ has better power scaling prospects than Nd:YVO_4 due to its (generally assumed) higher thermal conductivity, a detailed knowledge of thermal lensing effects as well as their reduction strategies is extremely important. This part of the research work addresses this need and characterizes the thermal lensing strength of a Nd:$GdVO_4$ laser under high power 912 nm pumping using a modified ABCD-matrix beam propagation technique that takes into account the beam quality factor (M^2) measurements [17].

It is worth to mention that thermal lensing strength would be different under different pumping conditions and predicting its behaviour in various experimental settings would be very helpful during the initial design of the laser setup. To this end, we performed numerical calculations and estimated the sensitivity factor of the thermal lens as well as the "generalized" thermo-optic coefficients based on our experimental data. Thereafter, the results of thermal lensing were compared with the experimental data of Nd:$GdVO_4$ lasers pumped at 808 nm and a Nd:YVO_4 laser pumped at 914 nm. Moreover, the FEA method was used to validate our experimental data.

3.2 Experimental setup

The experimental setup of the used Nd:$GdVO_4$ laser and thermal lensing measurement is shown in Fig. 3-1. The laser cavity consisted of a 20-mm-long (3×3 mm^2 cross-section) *a*-cut Nd:$GdVO_4$ crystal (1.5% doped) as a gain medium and 3 mirrors: a dichroic mirror (DM) with anti-reflection coating at 912 nm and high-reflection coating at 1063 nm, a concave mirror (M1) with radius of curvature of 500 mm and a flat output coupler with 15% transmission. The distances L1, L2 and L3 were 2.1, 33.7 and 51.3 cm, respectively. The laser crystal was wrapped in indium foil and water-cooled at 16 ℃ on its top and bottom surfaces. The system was pumped by a fiber-coupled laser diode operating around 912 nm (105 μm core diameter, NA = 0.22). The pumping light was focused into the center of the crystal with a spot diameter of ~390 μm. The ABCD matrix

calculations were used to design the cavity and the laser mode radius was set to be around 197 μm which ensured a reasonable mode matching between the pump and laser beams. In order to monitor the changes of the laser output beam characteristics at different pumping levels, a beam profiler with a lens was used in the system setup. A second DM after the output coupler was used to filter out the residual pump power.

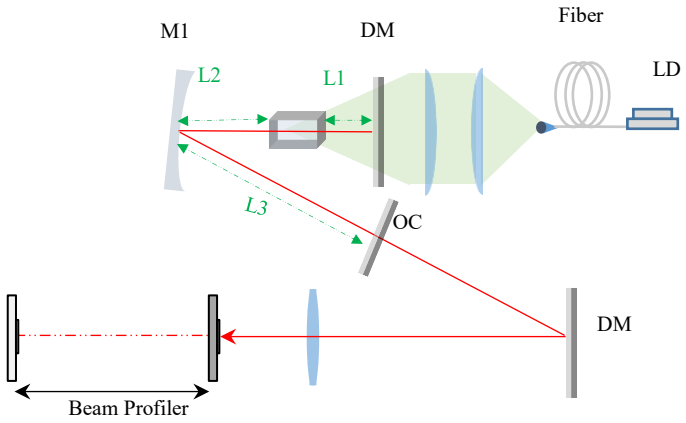

Fig. 3-1. Experimental setup of the Nd:$GdVO_4$ laser for the measurement of the thermal lensing effect.

3.3 Results and discussion

The measurement results for the laser output power versus the absorbed pump power are shown in Fig. 3-2-a. The maximum average output power of the Nd:$GdVO_4$ laser was measured to be ~11.3 W at 18.87 W of the absorbed pump power. This corresponds to the optical-to-optical efficiency and slope efficiency of 59.9% and 62.5%, respectively. The pump absorption coefficient was calculated to be ~ 0.7 cm^{-1}. The produced radiation was horizontally polarized (E // c-axis). The beam quality factor was measured at different output power levels and it was ~1.3 at the maximum output power. Fig. 3-2-b shows the output beam shape at several levels of output power.

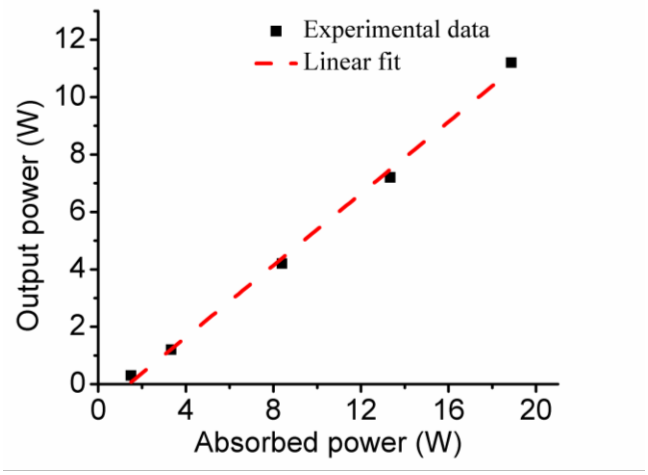

(a)

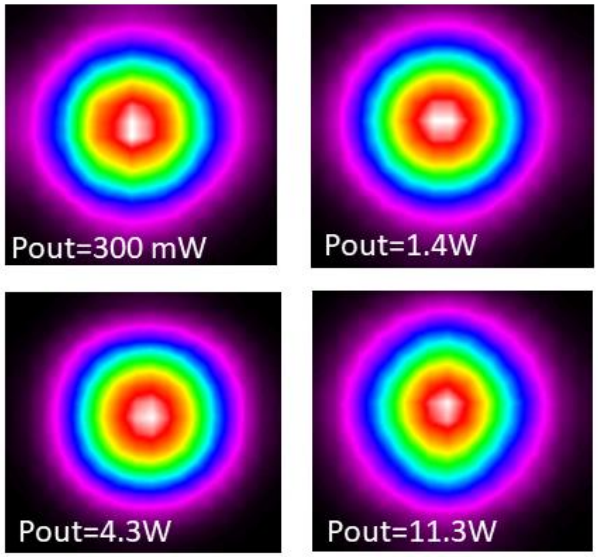

(b)

Fig. 3-2. (a) Output power versus the absorbed pump power. (b) Beam shapes at 0.3 W, 1.4 W, 4.3 W and 11.3 W of output power.

Characterization of the thermal lensing in this work was implemented using a modified ABCD-matrix beam propagation technique that takes into account the beam quality factor measurements [17]. Effective thermal lens was considered as a thin virtual lens at the center of the gain medium. A laser cavity with a variable lens at the center of the crystal was simulated by applying the ABCD matrix model. Knowing the experimentally measured output beam waist radius at different absorbed pump power levels, the focal length of the variable lens was adjusted

to get the simulated output beam with the same spatial characteristics. In order to get an accurate result, the beam quality factor that was used in the simulations was set to be equal to the experimentally measured value. The simulation process was performed with the commercial LASCAD software as described in detail elsewhere [17].

The measured dioptric power of the thermal lens at each pump power level is shown in Fig. 3-3. As expected, increasing the amount of absorbed pump power resulted in a more powerful thermal lensing strength. The maximum dioptric power of the induced thermal lens was found to be 9 m^{-1} at 18.87 W of the absorbed pump power.

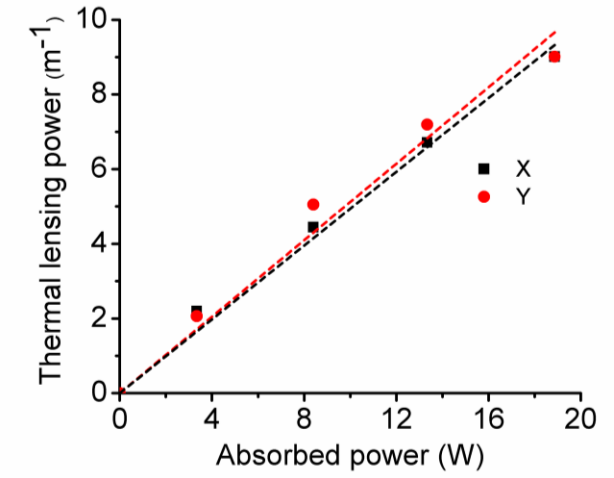

Fig. 3-3. Experimentally measured dioptric power of the thermal lens in the horizontal (X) and vertical (Y) directions for a 1063 nm Nd:$GdVO_4$ laser pumped at 912 nm.

To the best of our knowledge, this work is the first study of thermal lensing effect in Nd:$GdVO_4$ laser under the 912 nm direct diode pumping. Previous work on thermal lensing was performed under different experimental conditions such as different pumping wavelength (i.e. 808 nm) and different pump spot size, etc. [18-20]. Therefore, the direct comparison between the present data and previous experimental work would not be valid. To overcome this issue, a thermal lensing sensitivity factor can be used to compare the results under different experimental configurations as will be discussed below.

It is well known that the thermal lensing effect in solid-state lasers can be determined through the main three mechanisms: changes of the refractive index caused by its temperature dependence (d*n*/d*T*), variations of refractive index due to the thermally induced mechanical stress (photo-elastic effect, P_{PE}) and crystal end face bulging effect ($Q_{bulging}$) [1, 21]. In case of a laser diode pumping, the dioptric power D of thermal lensing can be expressed as [21, 22]:

$$D=\frac{P_{abs}\eta_h}{2\pi k_c w_p^2}\Delta\,, \qquad (3\text{-}1)$$

$$\Delta=\left(\frac{dn}{dT}+P_{PE}+Q_{bulging}\right), \qquad (3\text{-}2)$$

where P_{abs} is the absorbed pump power; ω_p is the pump waist radius; k_c is the thermal conductivity and Δ is the "generalized" thermo-optic coefficient representing the three main mechanisms responsible for thermal lensing effect. The η_h is the fractional heat load. Calculation of the Δ can help us to determine the thermal lensing strength in various experimental conditions (P_{abs}, ω_p, λ_p, etc.). This can be very helpful for designing purposes and also for comparing the current data with the other results which were not produced under the same pumping conditions.

Based on Eq. 3-1, the thermal lensing sensitivity factor can be written as [23]:

$$M=\frac{dD}{dP_{abs}}=\frac{\eta_h}{2\pi k_c w_p^2}\,\Delta\,, \qquad (3\text{-}3),$$

which is the slope of the thermal lensing dioptric power dependence on the absorbed pump power. Using the experimental data presented in Fig. 3-3, the average sensitivity factor *M* for both axes was calculated to be equal to 0.503 m^{-1}/W. This means that a 1 W increase in the absorbed pump power results in around 0.503 m^{-1} increase in the dioptric power of the induced thermal lens. Considering the *M* = 0.503 m^{-1}/W and η_h = 14.2% for the 1063 nm Nd:$GdVO_4$ laser with 912 nm pumping, thermal conductivity of ~10.75 W/m/K [24] and ω_p=197 μm, the Δ can be calculated from the Eq. 3-3 to be ~ 9.28×10^{-6} K^{-1} for our experimental conditions. With the known value of

Δ and other parameters, the pump spot size in Eq. 3-3 can be treated as a variable and the sensitivity factor can be estimated for any values of the pump radius ω_p. The dependence of the sensitivity factor on the pump beam waist radius for the 912 nm pumping was calculated and demonstrated in Fig. 3-4 (lower black curve). The experimental conditions of the developed laser are marked by a dot. As can be seen, the pump spot size has a great influence on the strength of thermal lensing and larger pump spot area results in smaller dioptric power of thermal lensing. However, it should be taken into account that this reduction in thermal lensing has an adverse effect on the laser threshold pump power (see equation 2-7 in chapter 2).

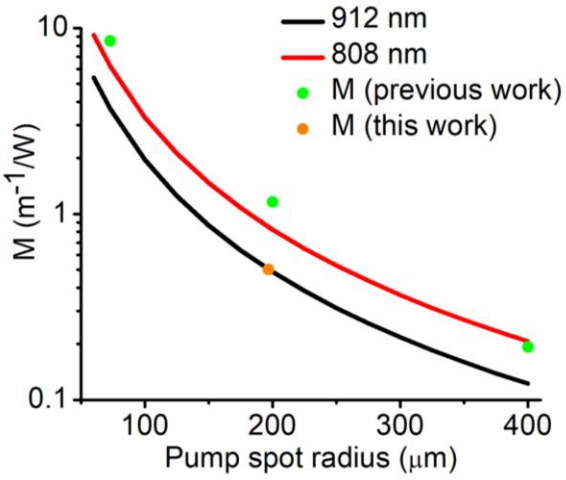

Fig. 3-4. Thermal lensing sensitivity factors versus pump spot radius for Nd:$GdVO_4$ lasers. Black and red curves: numerical calculation of M at various pump spot sizes with 912 nm and 808 nm pumping, respectively. Brown dot: M measured in the present work. Green dots: M measured under the 808 nm pumping [18-20].

Equation 3-3 may be used to approximately calculate the thermal lensing strength at various pumping wavelengths. Assuming similar values of Δ under the 808 nm and 912 nm pumping, variation of the pumping wavelength in Eq. 3-3 would modify the η_h value. Considering this change, the dependence of the sensitivity factor on the pump beam spot size radius was calculated for 808 nm pump wavelength and is displayed in Fig. 3-4 (upper red curve). As

expected, the values of the sensitivity factor (and hence thermal lens) are higher due to the higher quantum defect.

In addition, the thermal lensing sensitivity factor of the Nd:$GdVO_4$ laser under the 808 nm pumping were obtained from a set of experimental data given in [18-20], and were included in Fig. 3-4 as green dots. Comparing to the approximated behaviour of the thermal lens at 808 nm (which was obtained based on our experimental data under 912 nm pumping (brown dot in Fig. 3-4)), a reasonable agreement could be observed. This comparison validates our numerical approximation and also confirms that pumping of the laser at 912 nm instead of 808 nm reduces the thermal lensing strength by more than a factor of two.

Recently, the thermal lensing measurements in a 3×3×12-mm-long 0.5% doped Nd:YVO_4 crystal which was pumped at 914 nm with a spot size radius of 275 μm were reported [15]. The sensitivity factor was measured there was ~ 0.6 m^{-1}/W. Based on the data of Fig. 3-4, the sensitivity factor of the Nd:$GdVO_4$ laser in the present work can be estimated to be ~ 0.258 m^{-1}/W for the same pump spot size radius (275 μm). Therefore, Nd:$GdVO_4$ exhibits a much better thermal behavior. This is in favour of its better thermal conductivity in comparison with that of Nd:YVO_4 and adds to the still ongoing debate on this topic [25-27]. At the same time, it should be noticed that the aforementioned gain media possess different lengths and doping concentrations and the comparison stated here is an approximation.

It is worth mentioning that despite numerous work on characterization of the Nd:$GdVO_4$ crystal, there is still a great uncertainty on the true values of some of its important parameters such as thermo-optic coefficient (dn/dT) [19, 28-31]. In this context, the sign and magnitude of the dn/dT may be approximately estimated from Eq. 3-2 using the obtained value of Δ. In diode end-pumped lasers the photo-elastic effect is fairly small and for simplicity it may be ignored. Next,

the $Q_{bulging}$ term can be as estimated as $(1+v)(n-1)\alpha$ [21, 22], where n_e is the refractive index (~2.19 [24]); v is Poisson ratio (0.33 [32]) and α is the thermal expansion coefficient in the direction of light propagation (1.19×10^6 K^{-1} [28]). Using the corresponding data for the n_e, v and α, the $Q_{bulging}$ term will be equal to 1.88×10^{-6} K^{-1} and based on the obtained value of Δ (9.28×10^{-6} K^{-1}), the dn_e/dT can be calculated to be $\sim 7.4 \times 10^{-6}$ K^{-1}. If we compare the obtained dn_e/dT value with other reported data ($1.7\text{-}9.9 \times 10^{-6}$ K^{-1}) [19, 28-31], it shows that our approximated value is quite reasonable.

Furthermore, we also used the FEA method to validate our experimental data. FEA simulation was performed by the commercially available LASCAD software under conditions similar to the experimental ones (i.e. crystal and cooling geometry, pump spot size, absorbed pump power level, etc.). In addition to the pumping characteristics, thermo-optic effect and surface deformation were also considered in the simulation. The dn_e/dT values were selected from [30]. Fig. 3-5-a shows dioptric power of thermal lensing obtained by the FEA results as well as the experimental data from Fig. 3-3. The average sensitivity factor of the simulated thermal lensing can be calculated as 0.485 m^{-1}/W. The reasonable agreement between these results confirms our experimental work. The slight discrepancy can be attributed to the values of the input data that have been used in the simulation such as the dn_e/dT and thermal conductivity. An example of the temperature profile of the Nd:$GdVO_4$ crystal under pumping power of 18.87 W at 912 nm is illustrated in Fig. 3-5-b. A large spread of heat load in the crystal is the result of low pump absorption coefficient at 912 nm. As a result, the input surface area that was illuminated by the pump radiation had a temperature rise of only 9.2 K with respect to the heatsink, thus leading to the reduced contribution of surface bulging to thermal lensing.

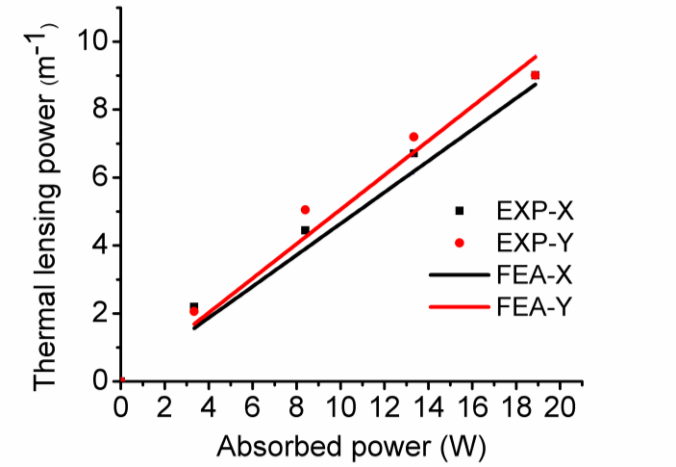

(a)

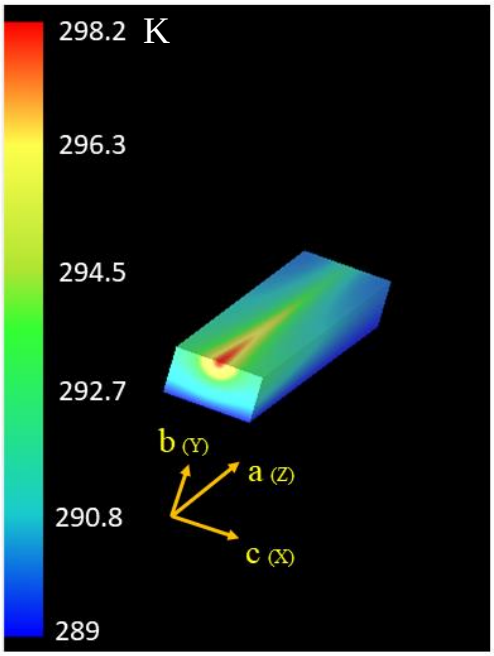

(b)

Fig. 3-5. (a) Dioptric power of thermal lensing obtained by FEA simulation (lines) as well as experimental data from Fig. 3-3 (dots). X and Y directions correspond to the *c*- and *b*- axes in FEA simulation, respectively. (b) Temperature profile of the Nd:$GdVO_4$ crystal for absorbed pump power of 18.87 W. A lower half of the crystal is shown. The *a*- and *c*-axes in the FEA model coincide with the corresponding axes and their orientation of the used crystal.

3.4 Conclusion

To conclude, experimental characterization of thermal lensing strength of a 1063 nm Nd:$GdVO_4$ laser in-band pumped at 912 nm was presented. The optical power of the thermal lens was varied linearly with the absorbed pump power and its sensitivity factor was as small as M = 0.503 m^{-1}/W. The obtained results showed a good agreement with finite element analysis simulation data. The experimental value of sensitivity factor enabled us to extend the numerical calculations of thermal lensing to various pump spot sizes and pump wavelengths. A comparison with previous data at 808 and 912 nm pump wavelengths showed excellent agreement with the model. It was also shown that the pump wavelength of 912 nm results in a factor of two lower thermal lensing when compared to the standard pump wavelength at 808 nm. Furthermore, the thermal lensing strength in the Nd:$GdVO_4$ laser with 912 nm pumping was found to be more than two times weaker when compared to the Nd:YVO_4 laser pumped at 914 nm. This points out to the higher thermal conductivity of the Nd:$GdVO_4$ crystal. Therefore in-band pumping at 912 nm offers an attractive method for further output power scaling of continuous-wave and pulsed oscillators [33, 34] that are highly desirable for a variety of nonlinear optical experiments [35-37].

References

1. W. Koechner, *Solid-state Laser Engineering*, 6th ed. (Springer, 2006).
2. M. P. MacDonald, T. Graf, J. E. Balmer, and H. P. Weber, "Reducing thermal lensing in diode-pumped laser rods," Opt. Commun. **178**, 383–393 (2000).
3. Y. A. Yun, H. Wei, L. H. Qing, B. Yong, L. X. Chun, G. A. Cong, K. Y. Peng, C. D. Fu and X. Z. Yan, "Reducing Thermal Effect in End-Diode-Pumped Laser Crystal by Using a Novel Resonator," Chinese Phys. Lett. **22**, 607–610 (2005).

4. X. Délen, F. Balembois, O. Musset, and P. Georges, “Characteristics of laser operation at 1064 nm in Nd:YVO_4 under diode pumping at 808 and 914 nm,” J. Opt. Soc. Am. B **28**, 52–57 (2011).
5. X. Ding, S.-J. Yin, C.-P. Shi, X. Li, B. Li, Q. Sheng, X.-Y. Yu, W.-Q. Wen, and J.-Q. Yao, “High efficiency 1342 nm Nd:YVO_4 laser in-band pumped at 914 nm,” Opt. Express **19**, 14315–14320 (2011).
6. J. Gao, X. Yu, X. D. Li, F. Chen, K. Zhang, R. P. Yan, J. H. Yu, and Y. Z. Wang, “456-nm deep-blue laser generation by intracavity frequency doubling of Nd:$GdVO_4$ under 879-nm diode pumping,” Laser Phys. **19**, 111–114 (2009).
7. Y. L. Li, J. Y. Liu, and Y. C. Zhang, “High efficiency 1341 nm Nd:$GdVO_4$ laser in-band pumped at 912 nm,” Laser Phys. **22**, 547–549 (2012).
8. Y.-F. Lü, J. Xia, J.-G. Wang, G.-C. Sun, X.-H. Zhang, A.-F. Zhang, X.-D. Yin, L. Bao, and H. Quan, “High-efficiency Nd:$GdVO_4$ laser at 1341 nm under 880 nm diode laser pumping into the emitting level,” Opt. Commun. **282**, 3565–3567 (2009).
9. V. Lupei, N. Pavel, Y. Sato, and T. Taira, “Highly efficient 1063-nm continuous-wave laser emission in Nd:$GdVO_4$,” Opt. Lett. **28**, 2366–2368 (2003).
10. J. L. Ma, B. Xiong, L. Guo, P. F. Zhao, L. Zhang, X. C. Lin, J. M. Li, and Q. D. Duanmu, “Low heat and high efficiency Nd:$GdVO_4$ laser pumped by 913 nm,” Laser Phys. Lett. **7**, 579–582 (2010).
11. N. Pavel, T. Dascalu, G. Salamu, O. Sandu, A. Leca, and V. Lupei, “Q-switched Nd lasers pumped directly into the $^4F_{3/2}$ emitting level,” Opt. Commun. **282**, 4749–4754 (2009).
12. D. Sangla, M. Castaing, F. Balembois, and P. Georges, “Highly efficient Nd:YVO_4 laser by direct in-band diode pumping at 914 nm,” Opt. Lett. **34**, 2159–2161 (2009).

13. H. J. Zhang, L. Zhu, X. L. Meng, Z. H. Yang, C. Q. Wang, W. T. Yu, Y. T. Chow, and M. K. Lu, "Thermal and Laser Properties of Nd:YVO_4 Crystal," Cryst. Res. Technol. **34**, 1011–1016 (1999).
14. T. Waritanant and A. Major, "High efficiency passively mode-locked Nd:YVO_4 laser with direct in-band pumping at 914 nm," Opt. Express **24**, 12851–12855 (2016).
15. T. Waritanant and A. Major, "Thermal lensing in Nd:YVO_4 laser with in-band pumping at 914 nm," Appl. Phys. B **122**, 135 (2016).
16. T. Waritanant and A. Major, "Diode-pumped Nd:YVO_4 laser with discrete multi-wavelength tunability and high efficiency," Opt. Lett. **42**, 1149–1152 (2017).
17. H. Mirzaeian, S. Manjooran, and A. Major, "A simple technique for accurate characterization of thermal lens in solid state lasers," Proc. SPIE **9288**, 928802 (2014).
18. H. Zhang, J. Liu, J. Wang, C. Wang, L. Zhu, Z. Shao, X. Meng, X. Hu, M. Jiang, and Y. T. Chow, "Characterization of the laser crystal Nd:$GdVO_4$," J. Opt. Soc. Am. B **19**, 18–27 (2002).
19. P. K. Mukhopadhyay, A. Nautiyal, P. K. Gupta, K. Ranganathan, J. George, S. K. Sharma, T. P. S. Nathan, "Experimental determination of the thermo-optic coefficient (dn /dT) and the effective stimulated emission cross-section (σ_e) of an a -axis cut 1.-at. % doped Nd:$GdVO_4$ crystal at 1.06 μm wavelength," Appl. Phys. B **77**, 81–87 (2003).
20. T. Omatsu, M. Okida, A. Lee and H. M. Pask, "Thermal lensing in a diode-end-pumped continuous-wave self-Raman Nd-doped $GdVO_4$ laser," Appl. Phys. B **108**, 73-79 (2012).
21. S. Chénais, F. Druon, S. Forget, F. Balembois, and P. Georges, "On thermal effects in solid-state lasers: The case of ytterbium-doped materials," Prog. Quantum Electron. **30**, 89–153 (2006).

22. P. A. Loiko, K. V. Yumashev, V. N. Matrosov, and N. V. Kuleshov, “Dispersion and anisotropy of thermo-optic coefficients in tetragonal $GdVO_4$ and YVO_4 laser host crystals,” Appl. Opt. **52**, 698–705 (2013).
23. P. Loiko, S. Manjooran, K. Yumashev, and A. Major, “Polarization anisotropy of thermal lens in Yb:$KY(WO_4)_2$ laser crystal under high-power diode pumping,” Appl. Opt. **56**, 2937– 2945 (2017).
24. L. J. Qin, X. L. Meng, H. Y. Shen, L. Zhu, B. C. Xu, L. X. Huang, H. R. Xia, P. Zhao, and G. Zheng, “Thermal conductivity and refractive indices of Nd:$GdVO_4$ crystals,” Cryst. Res. Technol. **38**, 793–797 (2003).
25. J. Didierjean, E. Herault, F. Balembois, and P. Georges, “Thermal conductivity measurements of laser crystals by infrared thermography. Application to Nd:doped crystals,” Opt. Express **16**, 8995–9010 (2008).
26. Y. Sato and T. Taira, “The studies of thermal conductivity in $GdVO_4$, YVO_4, and $Y_3Al_5O_{12}$ measured by quasi-one-dimensional flash method,” Opt. Express **14**, 10528–10536 (2006).
27. J. Morikawa, C. Leong, T. Hashimoto, T. Ogawa, Y. Urata, S. Wada, M. Higuchi, and J. Takahashi, “Thermal conductivity/diffusivity of Nd^{3+} doped $GdVO_4$, YVO_4, $LuVO_4$, and $Y_3Al_5O_{12}$ by temperature wave analysis,” J. Appl. Phys. **103**, 063522 (2008).
28. Y. Sato and T. Taira, “Highly accurate interferometric evaluation of thermal expansion and dn/dT of optical materials,” Opt. Mater. Express **4**, 876–888 (2014).
29. P. A. Loiko, K. V Yumashev, V. N. Matrosov, and N. V Kuleshov, “Dispersion and anisotropy of thermo-optic coefficients in tetragonal $GdVO_4$ and YVO_4 laser host crystals: erratum,” Appl. Opt. **54** 4820–4822 (2015).

30. D. E. Zelmon, J. J. Lee, K. M. Currin, J. M. Northridge, and D. Perlov, “Revisiting the optical properties of Nd doped yttrium orthovanadate,” Appl. Opt. **49**, 644-647 (2010).
31. H. Y. Shen, X. L. Meng, G. Zhang, J. J. Qin, W. Liu, L. Zhu, C. H. Huang, L. X. Huang, and M. Wei, “Sellmeier’s equation and the expression of the thermal refractive-index coefficient for a $Nd_{0.007}Gd_{0.993}VO_4$ crystal,” Appl. Opt. **43**, 955–960 (2004).
32. X. Peng, A. Asundi, Y. Chen, and Z. Xiong, “Study of the mechanical properties of Nd:YVO_4 crystal by use of laser interferometry and finite-element analysis,” Appl. Opt. **40**, 1396–1403 (2001).
33. Md. Z. E. Halim, R. C. Talukder, T. Waritanant, and A. Major, “Passive mode locking of a Nd:KGW laser with hot-band diode pumping,” Laser Phys. Lett. **13**, 105003 (2016).
34. T. Waritanant and A. Major, “Discretely selectable multiwavelength operation of a semiconductor saturable absorber mirror mode-locked Nd:YVO_4 laser,” Opt. Lett. **42**, 3331–3334 (2017).
35. R. Akbari and A. Major, “Optical, spectral and phase-matching properties of BIBO, BBO and LBO crystals for optical parametric oscillation in the visible and near-infrared wavelength ranges,” Laser Phys. **23**, 35401 (2013).
36. S. Manjooran, H. Zhao, I. T. Lima, and A. Major, “Phase-matching properties of PPKTP, MgO:PPSLT and MgO:PPcLN for ultrafast optical parametric oscillation in the visible and near-infrared ranges with green pump,” Laser Phys. **22**, 1325–1330 (2012).
37. A. Major, K. Sukhoy, H. Zhao, and I. T. Lima Jr, “Green sub-nanosecond microchip laser based on BiBO crystals”, Laser Phys. **21**(1), 57–60 (2011).

Chapter 4 – High power and beam quality continuous-wave Nd:$GdVO_4$ laser in-band diode-pumped at 912 nm[1]

As discussed in chapters 2 and 3, high power operation of solid-state lasers is highly desirable, however, it is usually limited by the thermal lensing effect [1]. Unlike the Nd:YVO_4 crystal, high power operation of the Nd:$GdVO_4$ laser crystal under 912 nm pumping was not demonstrated up to date. In this chapter we examined this issue and investigated high power performance of the Nd:$GdVO_4$ laser.

4.1 Introduction

It was discussed in chapter 3 that pumping of the Nd:YVO_4 and Nd:$GdVO_4$ crystal at absorption lines with long wavelengths (around 900 nm) has the advantages of significant reduction in quantum defect (and therefore thermal lensing effect) and enhancement of the theoretical upper limit of slope efficiency of a laser system [2-13]. Slope efficiencies of up to 80.7% in the continuous-wave [3] and up to 77.1% in the mode-locked regimes [14] were reported for the Nd:YVO_4 lasers using an in-band diode pumping at 914 nm (maximum output powers were 11.5 W and 6.7 W, respectively). In addition, it was also shown that the strength of thermal lensing with 914 nm pumping is more than two times weaker than that with traditional 808 nm. Therefore, power scaling of the Nd-doped lasers based on in-band pumping around 900 nm is a promising alternative. Recently, a 33.8 W

[1] This chapter contains material from [M. Nadimi, T. Waritanant, and A. Major, *"High power and beam quality continuous-wave Nd:$GdVO_4$ laser in-band diode-pumped at 912 nm,"* Photonics Res. 5, 346-349 (2017)]. Reprinted with permission. © 2017 Chinese Laser Press. All rights reserved.

CW Nd:YVO_4 laser with optical-to-optical efficiency of 50% and threshold pump power of ~18 W was realized with 914 nm pumping [15].

Despite notable research on Nd:YVO_4 lasers pumped around 914 nm [3, 4, 12, 14, 15], there is only one proof-of-principle work on CW Nd:$GdVO_4$ lasers using this pumping scheme in which an output power of 3.35 W with slope efficiency of 81.2% was reported [10]. The full power scaling potential of the Nd:$GdVO_4$ laser crystal to produce high output power was not demonstrated up to date. In this chapter we addressed this issue and demonstrated a high power (~20 W) CW Nd:$GdVO_4$ laser with high output beam quality under the 912 nm diode pumping.

4.2 Experimental setup

The gain medium that was used in this work was 1.5 at.% doped 3×3×20 mm^3 a-cut Nd:$GdVO_4$ crystal (Castech) which was anti-reflection (AR) coated at the pump and laser wavelengths. The laser crystal was wrapped in indium foil and the top and bottom surfaces of the crystal were water-cooled at 16 °C to remove the heat. The gain medium was pumped at 912 nm by a fiber-coupled laser diode with 105 μm fiber core diameter and numerical aperture of 0.22. The laser diode had a spectral width of ~3 nm at half maximum and it was cooled using a thermoelectric cooler. The temperature of the laser diode was monitored using a built in thermistor and was set to operate at 25.6 °C by a digital temperature controller. By using a couple of focusing lenses, the pump beam was focused into the center of the gain medium with a spot size radius of ~263 μm. Pump absorption in the crystal was measured to be 70%.

The designed laser cavity consisted of 3 mirrors and it is shown in Fig. 4-1. M1 is a concave mirror (500 mm radius of curvature) and DM is the flat dichroic mirror with high reflectivity at the laser wavelength (1063 nm) and high transmission around 912 nm. The distances L1, L2 and L3 were 90, 355 and 290 mm, respectively. The cavity design was based on ABCD matrix calculations that also considered

the effect of thermal lensing. The laser mode size was calculated to be ~ 263 μm at the center of crystal which shows reasonable mode-matching with the pump beam. Furthermore, several output couplers (10-40%) were tested and the maximum output power was achieved with an output coupler with 25% transmission.

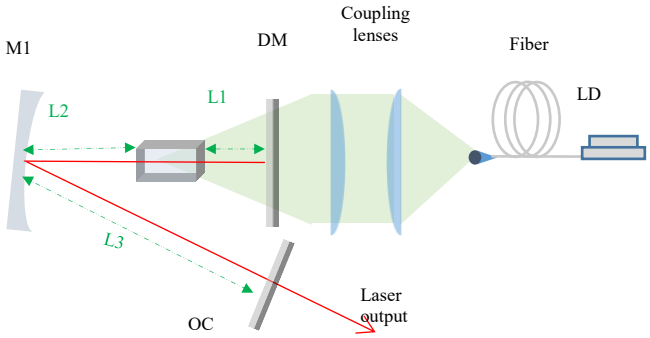

Fig. 4-1. Experimental setup for CW operation.

4.3 Results and discussion

Fig. 4-2-a represents the measurement results for the laser output power versus the absorbed pump power. The laser had a threshold of about 2.04 W of the absorbed pump power. The maximum output power reached 19.8 W at 33.4 W of the absorbed pump power. The radiation was linearly polarized with E//c-axis. This corresponds to the optical-to-optical and slope efficiencies of 59.3% and 62.7%, respectively. This, to the best of our knowledge, is the highest output power achieved to date from a Nd:$GdVO_4$ laser with in-band diode pumping at 912 nm and is almost six times higher than the previous maximum reported value [10].

Taking into account the slope efficiency of our system, it is obvious that the highest output power of the laser system was limited by the available pump power and not the thermal effects. The output power can be scaled by using a more powerful pumping source, longer crystal or multi-pass pumping scheme to

compensate for the lower absorption coefficient of Nd:$GdVO_4$ at 912 nm as compared to the other pump wavelengths.

Fig. 4-2-b shows the optical spectrum of the laser output. The peak value was at 1063.3 nm and the linewidth was measured to be around 0.08 nm.

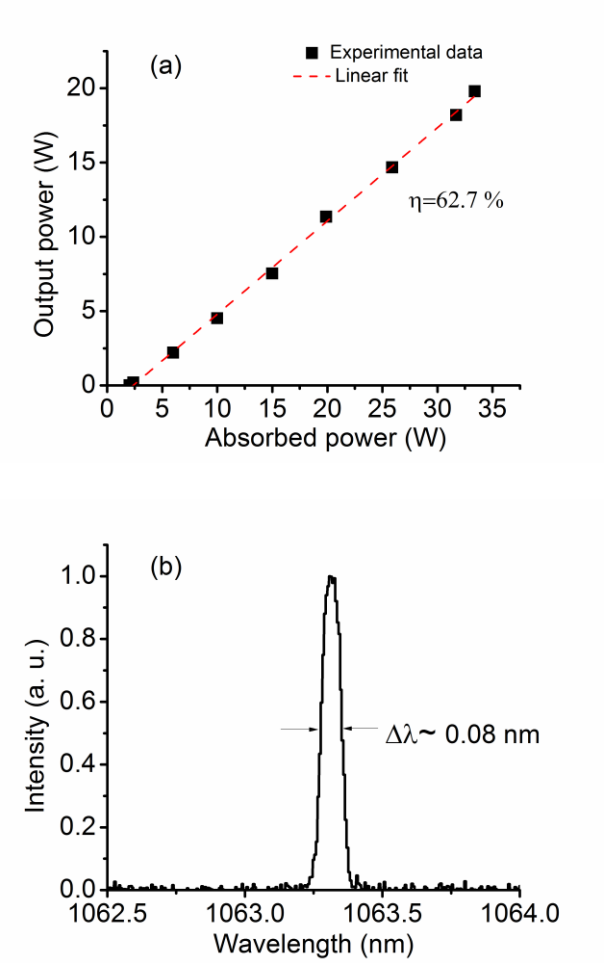

Fig. 4-2. (a) The output power versus pump power (with linear fit) and (b) laser spectrum.

The laser demonstrated an excellent output beam quality and TEM_{00} shape. The M^2 was measured by a beam profiler and was calculated to be 1.2 and 1.1 in the horizontal and vertical directions, respectively. The measured beam radii and the corresponding M^2 values at maximum output power are presented in Fig. 4-3, where also an output beam shape is displayed.

Considering the conventional 808 nm diode end pumping, the output power as high as 19.8 W was previously demonstrated [17]. The laser threshold was 3.6 W and optical and slope efficiencies were around 50.1% and 58.5%, respectively. However, the output beam quality was not diffraction limited (M^2 = 2.62). Comparing with the present results, we obtained the same output power, higher system efficiency, excellent beam quality, lower heating of the crystal and lower threshold.

There are also a few reports available on high power Nd:$GdVO_4$ lasers with high output beam quality pumped at 880 nm [18, 19]. To the best of our knowledge, the highest output power with this pump wavelength was 46 W with slope efficiency as high as 71.1% [18]. However, the laser used multiple composite crystals in the cavity and more complicated pumping setup (double-end pumping).

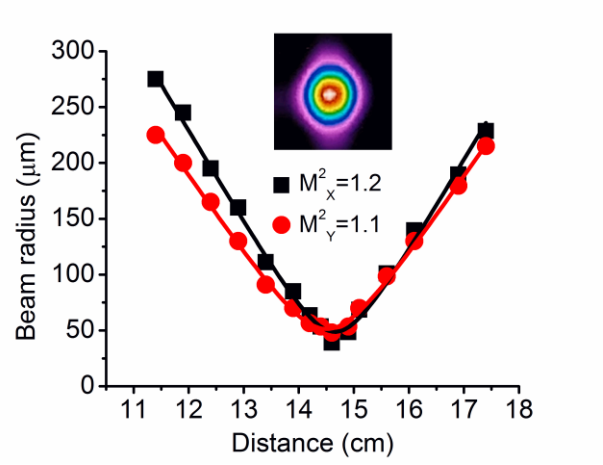

Fig. 4-3. Laser beam quality at 19.8 W of output power. Inset: transverse intensity profile of the laser beam.

The theoretical upper limit for slope efficiency with 912 nm pumping can be estimated to be around 86% which is higher than for 808 nm and 880 nm pump wavelengths. The lower efficiency of the present work could be attributed to the pump-mode overlap mismatch in the used 20 mm-long crystal. Despite the reasonable mode matching at the center of the gain medium, there was a mismatch between the pump and laser mode sizes at the end faces of the laser crystal (~340 μm versus ~260 μm, respectively) which reduced

the overall efficiency of the laser. The slope efficiency can be maximized by increasing the pump spot size provided that the available pump power can tolerate the increased threshold.

We also investigated the strength of thermal lensing at full power based on a modified ABCD-matrix analysis method [20]. At 33.4 W of absorbed pump power (19.8 W of output power), the focal length of the induced thermal lens was measured to be 120.3 mm and 112.3 mm in horizontal and vertical directions (corresponding to 8.3 and 8.9 diopters), respectively. Comparing these values with the measured thermal lensing of the 19.8 W Nd:$GdVO_4$ laser with 808 nm pumping [17], our system offers around two times weaker thermal lensing. Recently, a comprehensive study of thermal lensing effect in the 0.5 at.% Nd:YVO_4 crystal pumped at 914 nm was reported [12]. There, the strength of thermal lensing was obtained up to 6.55 W of the absorbed pump power. Thanks to the calculation of the sensitivity factor [21, 22] ($M \sim 0.6\ m^{-1}/W$), one can calculate the thermal lensing strength at ~33.4 W of the absorbed pump power to be above 20 diopters for Nd:YVO_4. Despite similar experimental conditions between this study and the previous work [12], the doping concentrations and pump absorption lengths are different and direct comparison between the obtained data is difficult and can be only approximate. However, it confirms the conclusion of Chapter 3 that the Nd:$GdVO_4$ laser crystal shows a much weaker thermal lensing effect (more than two times) under the equal amount of the absorbed pump power and similar pumping wavelength. Based on this data we are confident that the thermal conductivity of the Nd:$GdVO_4$ crystal is higher than that of the Nd:YVO_4 crystal, despite an ongoing debate on their true values [23-25]. Therefore, due to better thermal performance of the Nd:$GdVO_4$ crystal, its output power has the potential to be scaled up to the higher levels than with the Nd:YVO_4 crystal.

4.4 Conclusion

In summary, using a commercially available pump laser diode at 912 nm, a 19.8 W Nd:$GdVO_4$ laser with low threshold, high efficiency and excellent beam quality was demonstrated. The maximum

output power was almost six times higher than the previous maximum reported value with similar pumping wavelength. The strength of thermal lensing at full output power was measured to be an average of 8.6 diopters, indicating a factor of two reduction when compared to the Nd:$GdVO_4$ laser with 808 nm pumping or Nd:YVO_4 laser with 914 nm pumping. The highest output power of the laser system was limited only by the available pump power and not the thermal effects. Comparing to the theoretical maximum achievable slope efficiency of 86%, the lower efficiency of this work (62.7%) was attributed to the mismatch between the pump and laser mode sizes. Our results indicate that the 912 nm pumping wavelength is attractive for further power scaling of the Nd:$GdVO_4$ lasers. High power operation with excellent beam quality is attractive for mode locking [26-28], wavelength tunability [29] as well as efficient frequency conversion based, for example, on CW and pulsed optical parametric oscillators [30-33] or second harmonic generation of visible radiation [34] for pumping of vibronic lasers [35-37].

References

1. W. Koechner, *Solid-State Laser Engineering*, (Springer, 2006).
2. N. Pavel, T. Dascalu, G. Salamu, O. Sandu, A. Leca, and V. Lupei, "Q-switched Nd lasers pumped directly into the $^4F_{3/2}$ emitting level," Opt. Commun. **282**, 4749–4754 (2009).
3. D. Sangla, M. Castaing, F. Balembois, and P. Georges, "Highly efficient Nd:YVO_4 laser by direct in-band diode pumping at 914 nm," Opt. Lett. **34**, 2159–2161 (2009).
4. X. Délen, F. Balembois, O. Musset, and P. Georges, "Characteristics of laser operation at 1064 nm in Nd:YVO_4 under diode pumping at 808 and 914 nm," J. Opt. Soc. Am. B **28**, 52–57 (2011).
5. J. Gao, X. Yu, X. D. Li, F. Chen, K. Zhang, R. P. Yan, J. H. Yu, and Y. Z. Wang, "456-nm deep-blue laser generation by intracavity frequency doubling of Nd:$GdVO_4$ under 879-nm diode pumping," Laser Phys. **19**, 111–114 (2009).

6. Y.-F. Lü, J. Xia, J.-G. Wang, G.-C. Sun, X.-H. Zhang, A.-F. Zhang, X.-D. Yin, L. Bao, and H. Quan, "High-efficiency Nd:$GdVO_4$ laser at 1341 nm under 880 nm diode laser pumping into the emitting level," Opt. Commun. **282**, 3565–3567 (2009).
7. V. Lupei, N. Pavel, Y. Sato, and T. Taira, "Highly efficient 1063-nm continuous-wave laser emission in Nd:$GdVO_4$," Opt. Lett. **28**, 2366–2368 (2003).
8. H. J. Zhang, L. Zhu, X. L. Meng, Z. H. Yang, C. Q. Wang, W. T. Yu, Y. T. Chow, and M. K. Lu, "Thermal and Laser Properties of Nd:YVO_4 Crystal," Cryst. Res. Technol. **34**, 1011–1016 (1999).
9. Y. L. Li, J. Y. Liu, and Y. C. Zhang, "High efficiency 1341 nm Nd:$GdVO_4$ laser in-band pumped at 912 nm," Laser Phys. **22**, 547–549 (2012).
10. J. L. Ma, B. Xiong, L. Guo, P. F. Zhao, L. Zhang, X. C. Lin, J. M. Li, and Q. D. Duanmu, "Low heat and high efficiency Nd:$GdVO_4$ laser pumped by 913 nm," Laser Phys. Lett. **7**, 579–582 (2010).
11. X. Ding, S.-J. Yin, C.-P. Shi, X. Li, B. Li, Q. Sheng, X.-Y. Yu, W.-Q. Wen, and J.-Q. Yao, "High efficiency 1342 nm Nd:YVO_4 laser in-band pumped at 914 nm," Opt. Express **19**, 14315–14320 (2011).
12. T. Waritanant and A. Major, "Thermal lensing in Nd:YVO_4 laser with in-band pumping at 914 nm," Appl. Phys. B **122**, 135 (2016).
13. R. C. Talukder, Md. Z. E. Halim, T. Waritanant, and A. Major, "Multiwatt continuous wave Nd:KGW laser with hot-band diode pumping," Opt. Lett. **41**, 3810–3812 (2016).
14. T. Waritanant and A. Major, "High efficiency passively mode-locked Nd:YVO_4 laser with direct in-band pumping at 914 nm," Opt. Express **24**, 12851–12855 (2016).
15. L. Chang, C. Yang, X. J. Yi, Q. K. Ai, L. Y. Chen, M. Chen, G. Li, J. H. Yang, and Y. F.

Ma, “914 nm LD end-pumped 31.8 W high beam quality E-O Q-switched Nd:YVO_4 laser without intracavity polarizer,” Laser Phys. **22**, 1369–1372 (2012).

16. P. A. Studenikin, A. I. Zagumennyi, Y. D. Zavartsev, P. A. Popov, and I. A. Shcherbakov, “$GdVO_4$ as a new medium for solid-state lasers: some optical and thermal properties of crystals doped with Cd^{3+}, Tm^{3+}, and Er^{3+} ions,” Quantum Electron. **25**, 1162–1165 (1995).
17. J. Kong, D. Y. Tang, S. P. Ng, L. M. Zhao, L. J. Qin, and X. L. Meng, “High-power diode-end-pumped CW Nd:$GdVO_4$ laser,” Opt. Laser Technol. **37**, 51–54 (2004).
18. X. Li, X. Yu, F. Chen, R. Yan, M. luo, J. Yu, and D. Chen, “Power scaling of directly dual-end-pumped Nd:$GdVO_4$ laser using grown-together composite crystal,” Opt. Express **18**, 7407–7414 (2010).
19. H. Lin, J. Guo, P. Gao, H. Yu, and X. Liang, “High power, diffraction limited picosecond oscillator based on Nd:$GdVO_4$ bulk crystal with σ polarized in-band pumping,” Opt. Express **24**, 13957–13962 (2016).
20. H. Mirzaeian, S. Manjooran, and A. Major, “A simple technique for accurate characterization of thermal lens in solid state lasers,” Proc. SPIE **9288**, 928802 (2014).
21. H. Zhao and A. Major, “Orthogonally polarized dual-wavelength Yb:KGW laser induced by thermal lensing,” Appl. Phys. B **122**, 163 (2016).
22. P. Loiko, S. Manjooran, K. Yumashev, and A. Major, “Polarization anisotropy of thermal lens in Yb:$KY(WO_4)_2$ laser crystal under high-power diode pumping,” Appl. Opt. **56**, 2937–294 (2017).
23. J. Didierjean, E. Herault, F. Balembois, and P. Georges, “Thermal conductivity measurements of laser crystals by infrared thermography. Application to Nd:doped crystals,” Opt. Express **16**, 8995–9010 (2008).

24. J. Morikawa, C. Leong, T. Hashimoto, T. Ogawa, Y. Urata, S. Wada, M. Higuchi, and J. Takahashi, "Thermal conductivity/diffusivity of Nd^{3+} doped $GdVO_4$, YVO_4, $LuVO_4$, and $Y_3Al_5O_{12}$ by temperature wave analysis," J. Appl. Phys. **103**, 63522 (2008).
25. Y. Sato and T. Taira, "The studies of thermal conductivity in $GdVO_4$, YVO_4, and $Y_3Al_5O_{12}$ measured by quasi-one-dimensional flash method," Opt. Express **14**, 10528–10536 (2006).
26. Md. Z. E. Halim, R. C. Talukder, T. Waritanant, and A. Major, "Passive mode locking of a Nd:KGW laser with hot-band diode pumping," Laser Phys. Lett. **13**, 105003 (2016).
27. A. Major, L. Giniunas, N. Langford, A.I. Ferguson, D. Burns, E. Bente, and R. Danielius, "Saturable Bragg reflector-based continuous-wave mode locking of Yb:$KGd(WO_4)_2$ laser," J. Mod. Opt. **49**, 787–793 (2002).
28. A. Major, N. Langford, Th. Graf, D. Burns, and A.I. Ferguson, "Diode-pumped passively mode-locked Nd:$KGd(WO_4)_2$ laser with 1W average output power," Opt. Lett. **27**, 1478–1480 (2002).
29. T. Waritanant and A. Major, "Diode-pumped Nd:YVO_4 laser with discrete multi-wavelength tunability and high efficiency," Opt. Lett. **42**, 1149–1152 (2017).
30. H. Zhao, I. T. Lima, and A. Major, "Near-infrared properties of periodically poled $KTiOPO_4$ and stoichiometric MgO-doped $LiTaO_3$ crystals for high power optical parametric oscillation with femtosecond pulses," Laser Phys. **20**, 1404–1409 (2010).
31. R. Akbari and A. Major, "Optical, spectral and phase-matching properties of BIBO, BBO and LBO crystals for optical parametric oscillation in the visible and near-infrared wavelength ranges," Laser Phys. **23**, 35401 (2013).
32. S. Manjooran, H. Zhao, I. T. Lima, and A. Major, "Phase-matching properties of PPKTP, MgO:PPSLT and MgO:PPcLN for ultrafast optical parametric oscillation in the visible and

near-infrared ranges with green pump," Laser Phys. **22**, 1325–1330 (2012).

33. I. T. Lima, V. Kultavewuti, and A. Major, "Phasematching properties of congruent MgO-doped and undoped periodically poled $LiNbO_3$ for optical parametric oscillation with ultrafast excitation at 1 μm," Laser Phys. **20**, 270–275 (2010).
34. A. Major, D. Sandkuijl, and V. Barzda, "Efficient frequency doubling of a femtosecond Yb:KGW laser in a BiB_3O_6 crystal," Opt. Express **17**, 12039–12042 (2009).
35. K. Lamb, D. E. Spence, J. Hong, C. Yelland, and W. Sibbett, "All-solid-state self-mode-locked Ti:sapphire laser," Opt. Lett. **19**, 1864–1866 (1994).
36. S. Ghanbari, R. Akbari, and A. Major, "Femtosecond Kerr-lens mode-locked Alexandrite laser," Opt. Express **24**, 14836–14840 (2016).
37. S. Ghanbari and A. Major, "High power continuous-wave Alexandrite laser with green pump," Laser Phys. **26**, 75001 (2016).

Chapter 5 – Wavelength tuning of Nd:$GdVO_4$ laser[1]

In previous chapters the advantages of diode pumping at 912 nm were discussed and a high power CW Nd:$GdVO_4$ laser at 1063 nm was demonstrated. However, the emission spectrum of Nd:$GdVO_4$ also includes secondary emission bands at 1071 nm, 1083 nm and 1086 nm. In this chapter we examined the discrete multi-wavelength tuning and dual-wavelength operation of a Nd:$GdVO_4$ laser at the aforementioned wavelengths.

5.1 Discrete wavelength tuning of a diode-pumped Nd:$GdVO_4$ laser at 1063, 1071, 1083 and 1086 nm

5.1.1 Introduction

Apart from the main emission wavelength at 1063 nm, the emission spectrum of Nd:$GdVO_4$ crystal includes several other emission bands at 1071 nm, 1083 nm, and 1086 nm as shown in Fig. 5-1-a. These lines or their frequency-doubled versions (535-543 nm) have numerous applications in various areas of molecular and atomic studies [2-7] as well as medicine [8, 9]. Therefore, development of high power and efficient lasers at these wavelengths is important.

[1] The first part of this chapter contains material from [M. Nadimi, T. Waritanant, and A. Major, *"Discrete multi-wavelength tuning of a continuous wave diode-pumped Nd:$GdVO_4$ laser,"* Laser Phys. Lett. **15**, 055002 (2018)].

The second part of this chapter contains material from [M. Nadimi, and A. Major, *"Continuous-wave dual-wavelength operations of a diode-pumped Nd:$GdVO_4$ laser at 1063 & 1071 nm, 1063 & 1083 nm and 1083 &1086 nm,"* Laser Phys. **28**, 095001 (2018)].

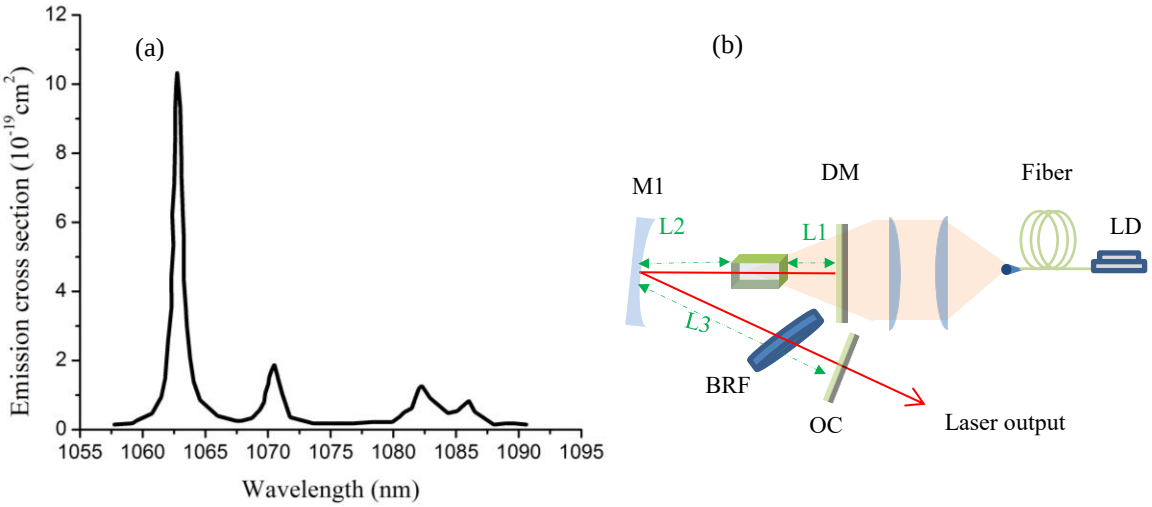

Fig. 5-1. (a) Emission spectrum of Nd:$GdVO_4$ (π-polarization) around the main transition at 1063 nm [1]. (b) Experimental configuration of wavelength-tunable Nd:$GdVO_4$ laser.

In chapter 4, efficient performance of a high power CW Nd:$GdVO_4$ laser at 1063 nm (the most intense spectral line) was demonstrated [10]. However, achieving laser performance at 1071 nm, 1083 nm, and 1086 nm would be much more challenging. The main reason for this is the fact that emission cross-section of Nd:$GdVO_4$ laser crystal at 1063 nm is more than 5 times higher than at the other wavelengths. Therefore, laser operation at nearby transitions is feasible only if the dominant 1063 nm wavelength is supressed. This can be achieved by implementing various optical elements within the laser setup such as specially coated mirrors, volume Bragg gratings (VBG) or etalons [11, 12]. Indeed, Nd:$GdVO_4$ lasers operating at 1083 nm and 1086 nm were previously reported by using custom coated mirrors. The maximum output powers at 1083 nm and 1086 nm were ~10.1 W [8] and ~2 W [5], respectively. This corresponds to an optical efficiency (with respect to the incident pump power) of 31.3% at 1083 nm and 33.3% at 1086 nm. In case of 1071 nm line, suppression of the main peak at 1063 nm by custom coated mirrors is very difficult because of its proximity. On the other hand, implementation of VBGs was proposed and ~1071 nm Nd:$GdVO_4$ laser with an output power ~0.38 W and optical efficiency of ~16.5% was reported

[11, 12]. In all of the aforementioned work on 1071 nm, 1083 nm and 1086 nm, the Nd:$GdVO_4$ lasers were pumped around 808 nm and produced up to two discrete wavelengths with a single setup, i.e. without exchange of the optical elements and re-alignment of a laser cavity. Development of a Nd:$GdVO_4$ laser which could provide selectable operation at any of the four emission lines using a single experimental setup would be very attractive but has not been reported yet.

In the following section we present our results on an efficient multi-watt Nd:$GdVO_4$ laser operating at four discrete wavelengths of 1063 nm, 1071 nm, 1083 nm, and 1086 nm. Wavelength selectivity was achieved using a single birefringent plate [13]. Comparing to the previous wavelength tuning experiments based on the Nd:$GdVO_4$ lasers, the present approach is much more simple as it only needs one laser setup to achieve CW operation at all four wavelengths.

5.1.2 Experimental setup

A schematic of the experimental setup is shown in Fig. 5-1-b. The laser active medium was a 20-mm-long 1.5 at.% doped Nd:$GdVO_4$ crystal which was antireflection coated at 912 nm and 1063 nm. The crystal was wrapped in indium foil and its top and bottom surfaces were water-cooled at 16 °C. The pump source was a 912 nm fiber-coupled laser diode with 105 μm fiber core diameter and numerical aperture of 0.22. By using collimating (f=40 mm) and focusing (f=150 mm) lenses, the pump beam was focused into the center of the gain medium with a spot size radius of ~197 μm. The designed laser cavity consisted of 3 mirrors and took into account the effect of thermal lensing [14]. M1 was a concave mirror (500 mm radius of curvature) and DM was the flat dichroic mirror with high reflectivity at 1063 nm and high transmission around 912 nm. Output coupler with 2.4% transmission in the 1040-1090 nm range was used to achieve the highest output power and efficiency for all of the four wavelengths. The distances L1, L2 and L3 were 21, 337

and 513 mm, respectively. In order to obtain a discrete wavelength tuning in this setup, a 4-mm-thick quartz birefringent plate (BRF) was used at the Brewster's angle between the M1 and OC. The BRF had its optic axis lying in the plane of the plate.

Birefringent plate in the cavity operates as the wavelength selective element by applying a wavelength dependent loss to the laser light. The incident polarized laser light passing through the BRF splits into the ordinary and extraordinary components and the phase retardation between them leads to the polarization rotation. At the Brewster's angle of incidence this introduces a wavelength dependent loss to the system through the Fresnel loss of the newly created s-polarization. The phase retardation depends on the birefringence of the material, its thickness and orientation of the incoming polarization with respect to the optical axis which can be conveniently changed by rotation of the filter about its surface normal.

At wavelengths where retardation is a full wave (i.e. incident p-polarization remains unchanged), the transmission of the filter will be maximum with no Fresnel reflection losses while all other wavelengths will experience losses. Therefore, the wavelength with minimum loss can be changed during the experiments by rotating the intracavity BRF about its surface normal. Theoretical details of BRF transmission profile are described elsewhere [13, 15-18]. Previous use of the same method with a diode-pumped Nd:YVO_4 laser demonstrated generation of three wavelengths in the 1064-1085 nm range [13].

5.1.3 Results and discussion

By rotating the intracavity BRF around its surface normal, laser operation was achieved at different wavelengths around 1063 nm, 1071 nm, 1083 nm, and 1086 nm. Fig. 5-2-a shows the measurement results for the laser output power versus the absorbed pump power at different laser wavelengths. The maximum output powers were 5.92 W, 5.66 W, 5.56 W and 3.98 W,

respectively. The output coupler (OC=2.4%) was optimized to get the maximum output powers at all lines. The optical-to-optical and slope efficiencies at the 1063 nm output were 44.2% and 44.3%, at the 1071 nm output 42.2% and 44.0%, at the 1083 nm output 41.5% and 43.4%, and at the 1086 nm output 34.6% and 39.3%, respectively. The M^2 of laser output was measured at the maximum output power for all of the mentioned wavelengths and it was below 1.6 in all cases. Fig. 5-2-b demonstrates the corresponding transverse beam intensity profiles. Furthermore, we also observed laser operation at 1084 nm (the fifth wavelength) with 3.12 W of output power. However, oscillation at this wavelength could be obtained only at one particular pump power level (11.5 W of absorbed pump power). Changing the pump power level resulted in switching of the laser to 1086 nm or 1083 nm. This behavior can be probably explained by poor discrimination of these more prominent transitions with respect to the 1084 nm line by the used BRF. The observed decrease in the laser output powers and efficiencies from 1063 nm to 1086 nm agrees well with the fact that these wavelengths have lower emission cross-sections (Fig. 5-1-a). In addition, operation at longer laser wavelengths results in slightly higher energy differences between the pump and laser photons (quantum defects) which in turn negatively affects their theoretical limit of slope efficiency [19].

The laser output spectra at the four wavelengths are shown in Fig. 5-3. The peak values were at 1063.2 nm, 1070.8 nm, 1082.5 nm and 1086.2 nm. The linewidths were measured to be around 0.08 nm and were limited by the resolution of the used spectrometer.

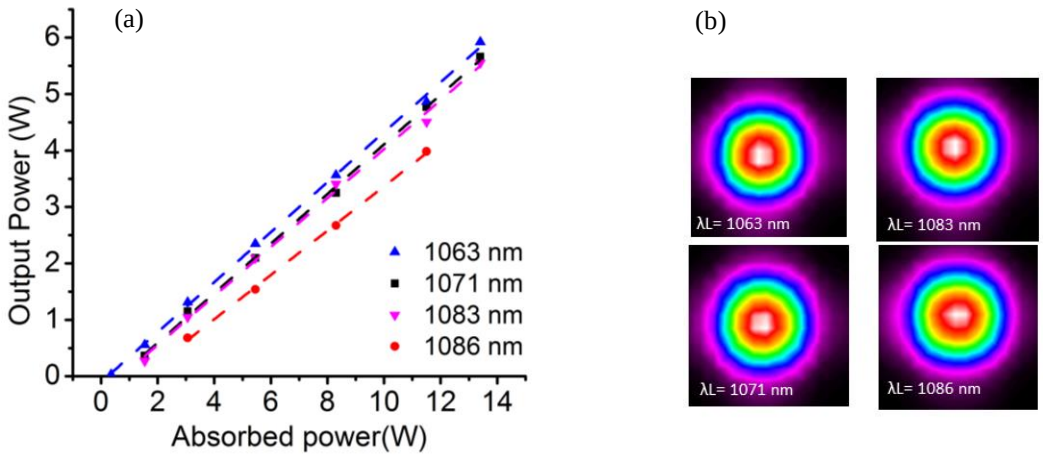

Fig. 5-2. (a) Measured output power versus absorbed power (with linear fits) at 1063 nm, 1071 nm, 1083 nm, and 1086 nm. (b) Transverse beam intensity profiles at the highest output powers for all wavelengths.

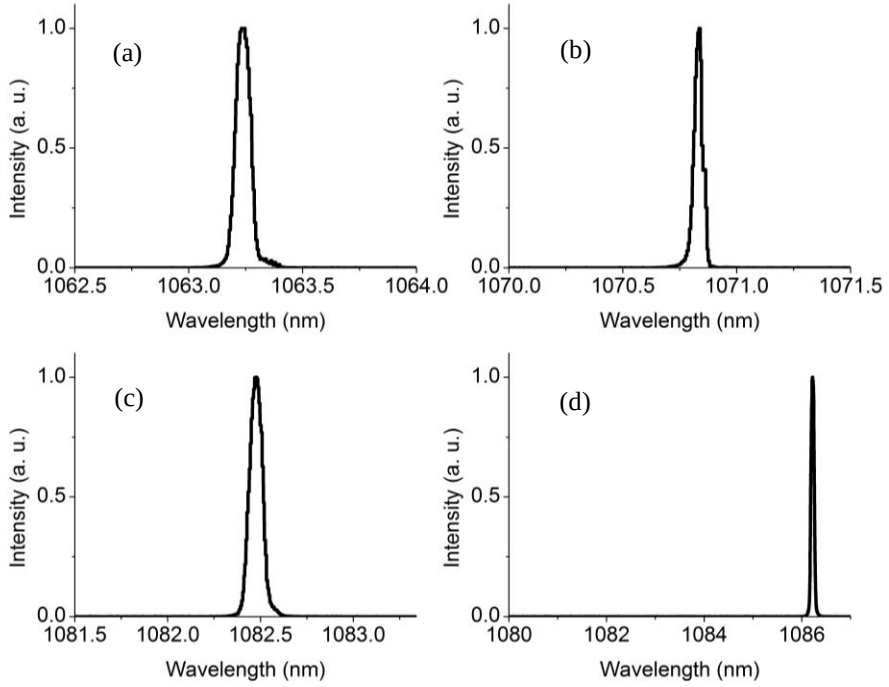

Fig. 5-3. Laser spectra at (a) 1063 nm, (b) 1071 nm, (c) 1083 nm, and d) 1086 nm.

In order to compare the present results with previous work, the performance of multi-wavelength Nd:$GdVO_4$ lasers operating in the 1070-1086 nm range is listed in Table 5-1. In addition, the data from other relevant neodymium-doped solid-state lasers were also included to diversify our comparison. On the other hand, single-wavelength laser operation results that were

previously reported only at the main emission lines of the $^4F_{3/2} \rightarrow {}^4I_{11/2}$ transition in the neodymium-doped crystals were not included in the table (such as 19.8 W Nd:$GdVO_4$ laser at 1063 nm [10]) as the main focus of the present work was on selectable multi-wavelength operation. Comparing the maximum output power with previous Nd:$GdVO_4$ lasers, the present work offers more than an order of magnitude higher output power at 1071 nm, while at 1086 nm it was doubled. Furthermore, higher efficiencies were achieved at 1071, 1083 and 1086 nm. Comparing with other Nd-doped lasers provided in Table 5-1, to the best of our knowledge, this work is the only one that achieved discrete wavelength operation at four wavelengths from a single setup and simultaneously offered high optical-to-optical and slope efficiencies. It should be noted that Nd:YAP crystal naturally has the strongest emission line around 1080 nm. On the other hand, demonstration of 5 wavelengths from the $^4F_{3/2} \rightarrow {}^4I_{11/2}$ transition of the Nd:Lu_2O_3 crystal required the use of three different output couplers. In addition, this laser operated mainly in the dual-wavelength rather than the single-wavelength regime and the output power did not exceed 1.5 W [20].

Considering the slope efficiency of the Nd:$GdVO_4$ laser at 1063 nm, 1071 nm, and 1083 in our system, the maximum output in the present work was limited by the amount of absorbed pump power rather than thermal lensing problems or instability due to gain competition between the different transitions. Therefore, higher output power could be achieved by using a more powerful pump source. An alternative way to generate similar wavelength-tunable radiation would be to use the well-known broadband gain media such as Yb-doped double tungstates [21-25] which, however, suffer from low emission cross-sections and relatively low thermal conductivity.

Table 5-1. Nd-doped lasers operating on $^4F_{3/2} \rightarrow {}^4F_{11/2}$ transition

Crystal	Wavelength (nm)	Output Power (W)	Slope Efficiency (%)	Opt-to-Opt Efficiency (%)	References
$Nd:GdVO_4$	1083 1086	3.4 2	30 -	28 33.3	[5]
$Nd:GdVO_4$	1063 1071 1083 1084* 1086	5.92 5.66 5.56 3.12 3.98	44.3 44.0 43.4 - 39.3	44.2 42.2 41.5 27.1 34.6	This work
$Nd:YVO_4$	1064 1073 1085	4.78 3.89 3.92	49.8 46.5 45.7	43.3 35.2 35.5	[13]
Nd:YAP	1073 1080 1084	5.2 6.5 0.57	35.8 - -	33.5 42.2 12.7	[26]
$Nd:Lu_2O_3$	1052+1056 1076+1080 1108	0.77 1.42 1.24	38.2 69.0 62.8	38 65.1 57.6	[20]

* Observed only at one specific pump power level.

5.1.4 Conclusion

In summary, to the best of our knowledge, the present work is the first demonstration of a discrete multi-wavelength tuning of a $Nd:GdVO_4$ laser using a simple cavity and a single birefringent filter plate. The laser achieved maximum output powers of 5.92 W, 5.66 W, 5.56 W and 3.98 W at 1063.2 nm, 1070.8 nm, 1082.5 nm, and 1086.2 nm, respectively. The slope efficiencies are superior than those previously reported for $Nd:GdVO_4$ lasers operating around 1071 nm, 1083 nm, and 1086 nm. Oscillation at 1084 nm was also observed. We believe that further power scaling is possible owing to the good thermo-optical properties of the $Nd:GdVO_4$ crystal and low quantum defect pumping employed in this work. Such multi-wavelength lasers can have potential applications in optical pumping of helium or similar molecular [6, 7] and atomic studies [2-5], and are attractive for mode locking [19, 27-29] and nonlinear frequency conversion through second harmonic, Raman or optical parametric generation [30-36].

5.2 Dual-wavelength operation of a diode-pumped Nd:$GdVO_4$ laser at the 1063 & 1071 nm, 1063 & 1083 nm and 1083 &1086 nm wavelength pairs

5.2.1 Introduction

Dual-wavelength lasers have attracted a strong interest in recent studies due to their application in different areas such as terahertz imaging and spectroscopy [37, 38]. Nd-doped solid-state laser crystals, which are well-known for their good spectral and mechanical properties, have proved to be great candidates for generation of dual-wavelength lasers [5, 39-50]. Dual-wavelength lasers within $^4F_{3/2}$–$^4I_{11/2}$ transition were previously demonstrated in many Nd-doped lasers such as Nd:YAG [51, 52], Nd:YLF [50], Nd:YVO_4 [53-56], Nd:YAP [26], Nd:LYSO [57] and Nd:$LuVO_4$ [46]. Comparing to these host materials, Nd:$GdVO_4$ crystal is another attractive choice due to its high absorption and emission cross-sections [58], high thermal conductivity [59] and polarized laser output. The latter is important for efficient frequency conversion [36, 60].

Based on the emission lines that was shown in Fig. 5-1-a, one can assume that dual-wavelength operation for Nd:$GdVO_4$ laser may be possible at three pairs of 1063 & 1083 nm, 1083 & 1086 and 1071 nm & 1083 nm. To achieve the dual-wavelength operation capabilities, the gain competition between the different emission lines should be effectively managed and similar lasing conditions for two different spectral lines must be obtained. This can be achieved by using an intracavity loss element in the system such as specifically coated mirrors, etalons and birefringent filters.

Dual-wavelength operation of Nd:$GdVO_4$ lasers has been previously reported at 1063 & 1083 nm [8] as well as 1083 & 1086 nm [5] wavelengths using specifically coated mirrors. However, to the best of our knowledge, the 1071 nm line has not been reported in dual-wavelength

operation so far. This might be due to its proximity to the intense emission at 1063 nm which makes a dual-wavelength operation much more challenging.

In the previous section of this chapter, discrete wavelength tuning of a CW Nd:$GdVO_4$ laser in the 1064-1085 nm range using a single birefringent filter was demonstrated [61]. Furthermore, recently, a dual-wavelength operation in Nd:YVO_4 laser at the two wavelength pairs of 1064 & 1073 nm and 1064 & 1085 nm using two BRFs in the cavity was reported [56]. In this part of the research, we were interested to examine dual-wavelength operation of a Nd:$GdVO_4$ laser at *three* possible wavelength pairs using a similar method. Like our experiments in chapter 3 and 4, 912 nm diode pumping was used to pump the Nd:$GdVO_4$ laser to minimise the thermal lensing effect and maximize its efficiency [10, 62-65].

5.2.2 Experimental setup

The experimental setup is similar to Fig. 5-1-b. Dual-wavelength laser operation can be achieved using an intracavity BRF. The wavelength-dependent selectivity characteristics of a BRF were briefly described in section 5.1.3. Previously, BRFs were used for demonstration of dual-wavelength Yb-ion [15, 66] and Alexandrite [67] lasers that are well-known for their broad gain bandwidths [68-70] and ability to generate ultrashort pulses [23, 71-73]. In this work, a 2-mm thick quartz BRF plate was used. It was placed in the cavity at the Brewster's angle between the M1 and OC (see Fig. 5-1-b). The used BRF had its optic axis parallel to the surface plane of the quartz plate.

5.2.3 Results and discussion

By fine adjustment of the BRF, dual-wavelength laser operation of the Nd:$GdVO_4$ laser at three different wavelength pairs of 1063 & 1071 nm, 1063 & 1083 nm and 1083 & 1086 nm was achieved. In all cases the wavelengths had polarization parallel to the *c*-axis of the crystal. Fig. 5-

4 shows the corresponding spectra for the first two pairs. In case of 1063 &1071 nm pair and at almost equal output power ratio (1:1 spectral amplitude ratio), the Nd:$GdVO_4$ laser achieved maximum output power of 2.52 W at 13.4 W of absorbed pump power. This corresponds to an optical-to-optical efficiency of 18.8%.

In case of 1063 & 1083 nm pair, 1.09 W of output power was obtained at 4.1 W of absorbed pump power which corresponds to an optical-to-optical efficiency of 26.6%. In case of 1083 & 1086 nm pair, the output power as high as 800 mW was achieved at 4.1 W of absorbed pump power which corresponds to 19.5% of optical-to-optical efficiency.

Rotation of the BRF or change in the absorbed pump power level could be used to adjust the power ratio between the two wavelengths or even to generate a single wavelength laser [13, 61]. Fig. 5-5 shows the output spectra for dual-wavelength laser at the third, 1083 & 1086 nm wavelength pair, with different power ratios. The same behaviour was observed for the other two pairs. Furthermore, we also observed a tri-wavelength laser operation at 1063 & 1071 & 1083 nm. However, the laser output was unstable and the output power ratio was not constant over the time. The typical spectrum is shown in Fig. 5-6.

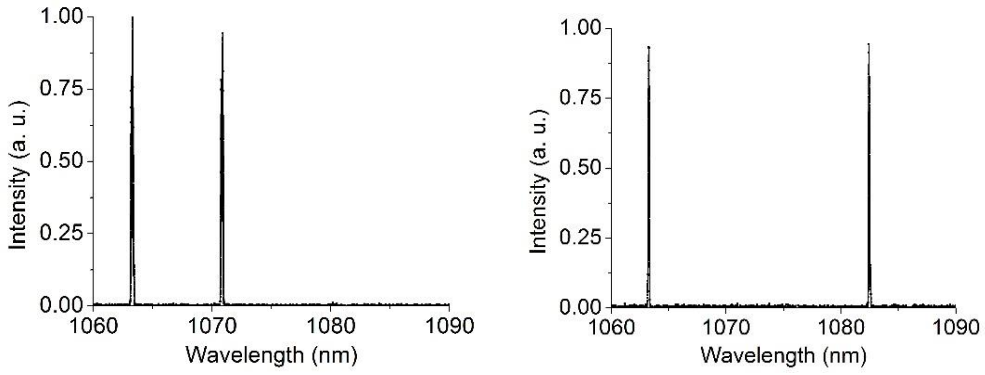

(a) (b)

Fig. 5-4. Dual-wavelength operation spectra: (a) at 1063 and 1071 nm, (b) at 1063 and 1083 nm.

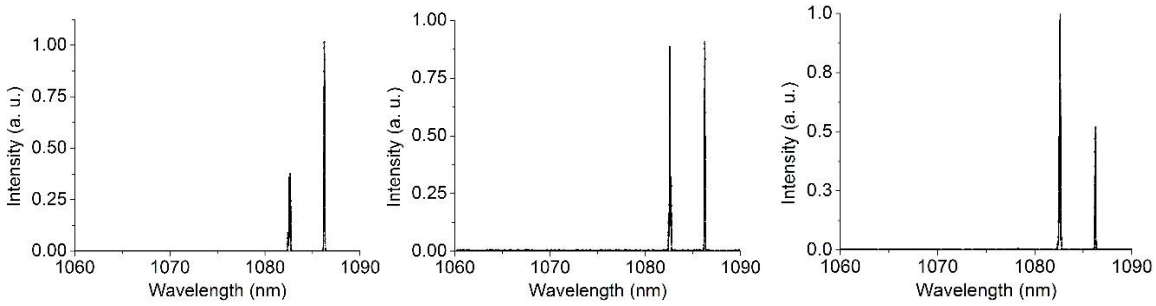

Fig. 5-5. Dual-wavelength operation spectra at 1083 and 1086 nm. (a), (b), and (c) show the control of power ratio between the two output wavelengths by changing the rotation angle of the BRF plate.

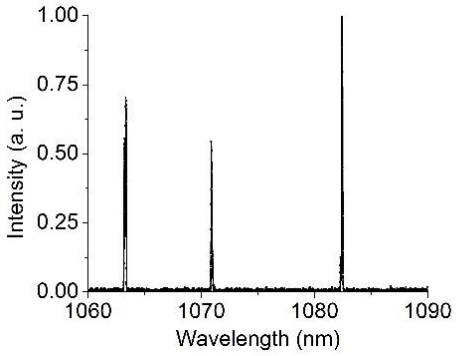

Fig. 5-6. Tri-wavelength laser spectrum at 1063, 1071 and 1083 nm at 0.88 W of output power.

To compare the present data with the previous reports, the performance of relevant dual-wavelength Nd-doped lasers in the 1.06-1.08 μm range is listed in table 5-2. To the best of our knowledge, this work is the first report on dual-wavelength operation of a Nd:$GdVO_4$ laser at 1063 & 1071 nm. Furthermore, it should be noted that the dual-wavelength operation at three pairs was achieved with a single setup without the need to realign the laser cavity or to exchange any of the optical elements. Previous dual-wavelength Nd:$GdVO_4$ lasers operating on the $^4F_{3/2} \rightarrow {}^4F_{11/2}$ transition usually operated only at one pair of wavelengths [5, 8, 74]. We achieved slightly higher optical-to-optical efficiency for 1063 & 1083 nm pair and almost twice lower optical-to-optical efficiency for 1083 & 1086 nm pair. The lower output power and efficiency of our results at 1083

& 1086 nm can be probably explained by the less optimum transmission of our output coupler for this specific pair.

In comparison to the recently reported 1064 & 1073 nm and 1064 & 1085 nm dual-wavelength Nd:YVO_4 laser [56], present work offers higher efficiency using a less complicated experimental setup (only one BRF was used in the cavity instead of two).

On the other hand, it should be considered that the main emission lines of the Nd:Lu_2O_3 and Nd:YAP crystals are located around 1076 and 1080 nm, respectively [20, 26]. Furthermore, demonstration of dual-wavelength laser operation from the $^4F_{3/2} \rightarrow {}^4I_{11/2}$ transition of the Nd:Lu_2O_3 crystal required the use of two different OCs and the intensity ratio at 1076 & 1080 nm was estimated to be ~2:1 and was not controllable. The high efficiency of the Nd:Lu_2O_3 laser can be explained by the diffraction limited pump radiation that was provided by a Ti:sapphire laser. Power scaling of such a complex pumping method, however, is very limited.

At the same time, it should be noted that the number of the produced wavelength pairs can be increased by using laser crystals with more rich emission spectra than Nd-ion doped vanadates. This, unfortunately, will negatively affect laser efficiency. For example, the Cr:Nd:GSGG laser was recently shown to produce 11 wavelength pairs around 1.06 μm but its optical efficiency for many of them was below 1% [18].

Table 5-2. Nd-doped dual-wavelength lasers with power ratio ~1:1 operating on $^4F_{3/2} \rightarrow {}^4F_{11/2}$ transition

Crystal	**Wavelength (nm)**	**Total Power (W)**	**Opt-to-Opt Efficiency (%)**	**References**
Nd:$GdVO_4$	1083/1086	~3	37.5	[5]
Nd:$GdVO_4$	1063/1083	~4	25	[8]
Nd:$GdVO_4$	1063/1071 1063/1083 1083/1086	2.52 1.09 0.80	18.8 26.6 19.5	This work
Nd:YVO_4	1064/1073 1064/1085	1.44 1.46	13 13.2	[56]
Nd:$LuVO_4$	1086/1089	1.5	17	[46]
Nd:$LiYF_4$	1047/1053	1.25	21.6	[50]
Nd:YAP	1072/1080 1073/1084 1079/1084	4.4 1.8 3.2	-	[26]
Nd:YAG	1064/1078	1.57	10.3	[52]
Nd:Lu_2O_3	1052/1056 1076/1080*	0.77 1.42	38.2 69.0	[20]

*Power ratio was estimated to be (~2:1). Laser was not diode-pumped.

5.2.4 Conclusion

In conclusion, we demonstrated a discretely tunable dual-wavelength operation of a Nd:$GdVO_4$ laser using a single BRF within the experimental setup. To the best of our knowledge, this is also the first demonstration of CW dual-wavelength operation of a diode-pumped Nd:$GdVO_4$ laser at 1063 nm and 1071 nm and also the first report on generation of three CW dual-wavelength laser pairs with adjustable power ratios within the $^4F_{3/2}$–$^4I_{11/2}$ transition from any of the Nd-ion doped vanadate lasers. Such dual-wavelength lasers are useful in THz generation applications (2-5 THz). Furthermore, an unstable tri-wavelength laser operation at 1063 nm & 1071 nm & 1083 nm was also observed. If multiple BRFs are to be used in a similar setup, stable tri-wavelength laser operation can be expected. Considering a low quantum defect 912 nm diode pumping scheme in this work, we believe that the maximum output power of the present setup can be increased by optimization of the BRF thickness and transmission of the output coupler at

different wavelengths as well as increasing the pump power. High power multi-wavelength lasers can be a very attractive alternative to more complex systems based on nonlinear frequency conversion [30-33].

References

1. Y. Sato and T. Taira, "Comparative study on the spectroscopic properties of Nd:$GdVO_4$ and Nd:YVO_4 with hybrid process," *IEEE J. Sel. Top. Quantum Electron.* **11**, 613–620 (2005).
2. A. D. Cronin, R. B. Warrington, S. K. Lamoreaux, and E. N. Fortson, "Studies of Electromagnetically Induced Transparency in Thallium Vapor and Possible Utility for Measuring Atomic Parity Nonconservation," Phys. Rev. Lett. **80**, 3719–3722 (1998).
3. N.-C. Shie, C.-Y. Chang, W.-F. Hsieh, Y.-W. Liu, and J.-T. Shy, "Frequency measurement of the $6P_{3/2} \rightarrow 7S_{1/2}$ transition of thallium," Phys. Rev. A **88**, 62513 (2013).
4. N.-C. Shie, S.-E. Chen, C.-Y. Chang, W.-F. Hsieh, and J.-T. Shy, "Absolute frequency measurements of the molecular iodine hyperfine transitions at 535 nm," J. Opt. Soc. Am. B **30**, 2022 (2013).
5. Y. F. Chen, M. L. Ku, and K. W. Su, "High-power efficient tunable Nd:$GdVO_4$ laser at 1083 nm.," Opt. Lett. **30**, 2107–2109 (2005).
6. L. D. Schearer and P. Tin, "Tunable lasers at 1080 nm for helium optical pumping," J. Appl. Phys. **68**, 943–949 (1990).
7. C. L. Bohler, "Low-noise Nd:$LaMgAl_{11}O_{19}$ laser for use in magnetometry," J. Appl. Phys. **66**, 4614–4620 (1989).

8. L. Chen, Z. Wang, H. Yu, S. Zhuang, S. Han, Y. Zhao, and X. Xu, "High-Power Single- and Dual-Wavelength Nd:$GdVO_4$ Lasers with Potential Application for the Treatment of Telangiectasia," Appl. Phys. Express, **5**, 112701 (2012).
9. N. Bouzari, S. C. Davis, and K. Nouri, "Laser treatment of keloids and hypertrophic scars," Int. J. Dermatol. **46**, 80–88 (2007).
10. M. Nadimi, T. Waritanant, and A. Major, "High power and beam quality continuous-wave Nd:$GdVO_4$ laser in-band diode-pumped at 912 nm," Photon. Res. **5**, 346–349 (2017).
11. Te-Yuan Chung, Chien-Jung Liao, Yu-Hung Lien, Sideny S. Yang, "Special Laser Wavelength Generation Using a Volume Bragg Grating as Nd:$GdVO_4$ Laser Mirror," Jpn. J. Appl. Phys. **49**, 62503 (2010).
12. N.-C. Shie, W.-F. Hsieh, and J.-T. Shy, "Single frequency 1070 nm Nd:$GdVO_4$ laser using a volume Bragg grating," Opt. Express **19**, 21109–21115 (2011).
13. T. Waritanant and A. Major, "Diode-pumped Nd:YVO_4 laser with discrete multi-wavelength tunability and high efficiency," Opt. Lett. **42**, 1149–1152 (2017).
14. H. Mirzaeian, S. Manjooran, and A. Major, "A simple technique for accurate characterization of thermal lens in solid state lasers," Proc. SPIE **9288**, 928802 (2014).
15. R. Akbari, H. Zhao, and A. Major, "High-power continuous-wave dual-wavelength operation of a diode-pumped Yb:KGW laser," Opt. Lett. **41**, 1601–1604 (2016).
16. S. Zhu, "Birefringent filter with tilted optic axis for tuning dye lasers: theory and design," Appl. Opt. **29**, 410–415 (1990).
17. K. Naganuma, G. Lenz, and E. P. Ippen, "Variable bandwidth birefringent filter for stable femtosecond lasers," IEEE J. Quantum Electron. **28**(10), 2142–2150 (1992).

18. U. Demirbas, R. Uecker, J. G. Fujimoto, and A. Leitenstorfer, “Multicolor lasers using birefringent filters: experimental demonstration with Cr:Nd:GSGG and Cr:LiSAF,” Opt. Express **25**, 2594–2607 (2017).
19. T. Waritanant and A. Major, “High efficiency passively mode-locked Nd:YVO_4 laser with direct in-band pumping at 914 nm,” Opt. Express **24**, 12851–12855 (2016).
20. P. V. Brunn, A. M. Heuer, L. Fornasiero, G. Huber, and C. Kränkel, “Efficient laser operation of Nd^{3+}: Lu_2O_3 at various wavelengths between 917 nm and 1463 nm,” Laser Phys. **26**, 84003 (2016).
21. A. Major, L. Giniunas, N. Langford, A.I. Ferguson, D. Burns, E. Bente, and R. Danielius, “Saturable Bragg reflector-based continuous-wave mode locking of Yb:$KGd(WO_4)_2$ laser,” J. Mod. Opt. **49**, 787–793 (2002).
22. R. Akbari, H. Zhao, K. A. Fedorova, E. U. Rafailov, and A. Major, “Quantum-dot saturable absorber and Kerr-lens mode-locked Yb:KGW laser with >450 kW of peak power,” Opt. Lett. 41, 3771–3774 (2016).
23. A. Major, R. Cisek, and V. Barzda, “Development of diode-pumped high average power continuous-wave and ultrashort pulse Yb:KGW lasers for nonlinear microscopy,” Proc. SPIE **6108**, 61080Y (2006).
24. R. Akbari, K. A. Fedorova, E. U. Rafailov, and A. Major, “Diode-pumped ultrafast Yb:KGW laser with 56 fs pulses and multi-100 kW peak power based on SESAM and Kerr-lens mode locking,” Appl. Phys. B **123**, 123 (2017).
25. H. Zhao and A. Major, “Megawatt peak power level sub-100 fs Yb:KGW oscillators,” Opt. Express **22**, 30425–30431 (2014).

26. Y. S. Tzeng, Y. J. Huang, C. Y. Tang, K. W. Su, W. D. Chen, G. Zhang, and Y. F. Chen, "High-power tunable single- and multi-wavelength diode-pumped Nd:YAP laser in the $^4F_{3/2} \rightarrow {}^4I_{11/2}$ transition," Opt. Express **21**, 26261–26268 (2013).
27. Md. Z. E. Halim, R. C. Talukder, T. Waritanant, and A. Major, "Passive mode locking of a Nd:KGW laser with hot-band diode pumping," Laser Phys. Lett. **13**, 105003 (2016).
28. T. Waritanant and A. Major, "Discretely selectable multiwavelength operation of a semiconductor saturable absorber mirror mode-locked Nd:YVO_4 laser," Opt. Lett. **42**, 3331–3334 (2017).
29. A. Major, N. Langford, T. Graf and A. I. Ferguson, "Additive-pulse mode locking of a diode-pumped Nd:$KGd(WO_4)_2$ laser," Appl. Phys. B **75**, 467–469 (2002).
30. H. Zhao, I.T. Lima, and A. Major, "Near-infrared properties of periodically poled KTiOPO4 and stoichiometric MgO-doped $LiTaO_3$ crystals for high power optical parametric oscillation with femtosecond pulses," Laser Phys. **20**, 1404–1409 (2010).
31. R. Akbari, A. Major, "Optical, spectral and phasematching properties of BIBO, BBO and LBO crystals for optical parametric oscillation in the visible and near-infrared wavelength ranges," Laser Phys. **23**, 035401 (2013).
32. S. Manjooran, H. Zhao, I.T. Lima, and A. Major, "Phasematching properties of PPKTP, MgO:PPSLT and MgO:PPcLN for ultrafast optical parametric oscillation in the visible and near-infrared ranges with green pump," Laser Phys. **22**, 1325–1330 (2012).
33. I.T. Lima, V. Kultavewuti, and A. Major, "Phasematching properties of congruent MgO-doped and undoped periodically poled $LiNbO_3$ for optical parametric oscillation with ultrafast excitation at 1 μm," Laser Phys. **20**, 270–275 (2010).

34. A. Major, D. Sandkuijl, and V. Barzda, “Efficient frequency doubling of a femtosecond Yb:KGW laser in a BiB_3O_6 crystal,” Opt. Express **17**, 12039–12042 (2009).

35. A. Major, J.S. Aitchison, P.W.E. Smith, N. Langford, A.I. Ferguson, “Efficient Raman shifting of high-energy picosecond pulses into the eye-safe 1.5 um spectral region using a $KGd(WO_4)_2$ crystal,” Opt. Lett. **30**, 421–423 (2005).

36. A. Major, K. Sukhoy, H. Zhao, and I. T. Lima Jr, “Green sub-nanosecond microchip laser based on BiBO crystals,” Laser Phys. **21**, 57–60 (2011).

37. A. Saha, A. Ray, S. Mukhopadhyay, N. Sinha, P. K. Datta, and P. K. Dutta, “Simultaneous multi-wavelength oscillation of Nd laser around 1.3 μm: A potential source for coherent terahertz generation,” Opt. Express **14,** 4721–4726 (2006).

38. J. B. Baxter and G. W. Guglietta, “Terahertz Spectroscopy,” Anal. Chem. **83**, 4342–4368 (2011).

39. C. Bethea, “Megawatt power at 1.318 μ in Nd^{3+}:YAG and simultaneous oscillation at both 1.06 and 1.318 μ,” IEEE J. Quantum Electron. **9**, 254–254 (1973).

40. H- Y. Shen, R. R. Zeng, Y- P. Zhou, G. F. Yu, C- H. Huang, Z- D. Zeng, W. J. Zhang, and Q. J. Ye, “Simultaneous multiple wavelength laser action in various neodymium host crystals,” IEEE J. Quantum Electron. **27**, 2315–2318 (1991).

41. H. Lin, W. Zhu, F. Xiong, and J. Ruan, “Simultaneous dual-wavelength Q-switched Nd:YAG laser at 1052 and 1073 nm,” Appl. Opt. **56**, 948–951 (2017).

42. Y. Lu, B. Zhang, E. Li, D. Xu, R. Zhou, X. Zhao, F. Ji, T. Zhang, P. Wang, and J. Yao, “High-power simultaneous dual-wavelength emission of an end-pumped Nd:YAG laser using the quasi-three-level and the four-level transition,” Opt. Commun. **262**, 241–245 (2006).

43. N. Pavel, “Simultaneous dual-wavelength emission at 0.90 and 1.06 μm in Nd-doped laser crystals,” Laser Phys. **20**, 215–221 (2010).

44. Y.-F. Chen, “cw dual-wavelength operation of a diode-end-pumped Nd:YVO_4 laser,” Appl. Phys. B **70**, 475–478 (2000).

45. J. L. He, J. Du, J. Sun, S. Liu, Y. X. Fan, H. T. Wang, L. H. Zhang, Y. Hang, “High efficiency single- and dual-wavelength Nd:$GdVO_4$ lasers pumped by a fiber-coupled diode,” Appl. Phys. B **79**, 301–304 (2004).

46. Y. P. Huang, C. Y. Cho, Y. J. Huang, and Y. F. Chen, “Orthogonally polarized dual-wavelength Nd:$LuVO_4$ laser at 1086 nm and 1089 nm,” Opt. Express **20** 5644–5651 (2012).

47. H. Yu, H. Zhang, Z. Wang, J. Wang, Y. Yu, Z.Shi, X. Zhang, and M. Jiang, “High-power dual-wavelength laser with disordered Nd:CNGG crystals,” Opt. Lett. **34**, 151–153 (2009).

48. H. Y. Shen, R. R. Zeng, Y. P. Zhou, G. F. Yu, C. H. Huang, Z. D. Zeng, W. J. Zhang, and Q. J. Ye, “Comparison of simultaneous multiple wavelength lasing in various neodymium host crystals at transitions from $^4F_{3/2} - {}^4I_{11/2}$ and $^4F_{3/2} - {}^4I_{13/2}$,” Appl. Phys. Lett. **56**, 1937–1938 (1990).

49. B. Xu, Y. Wang, Y. Cheng, H. Xu, Z. Cai, and R. Moncorgé, “Single- and multi-wavelength laser operation of a diode-pumped ND:GGG single crystal around 1.33 μm,” Opt. Commun. **345**, 111–115 (2015).

50. Z. Lin, Y. Wang, B. Xu, Y. Cheng, H. Xu, and Z. Cai, “Simultaneous dual-wavelength lasing at 1047 and 1053 nm and wavelength tuning to 1072 nm in a diode-pumped a -cut Nd:$LiYF_4$ laser,” Opt. Eng. **54**, 126114 (2015).

51. X. Z. Wang, Z. F. Wang, Y. K. Bu, L. J. Chen, G. X. Cai, and Z. P. Cai, "A 1064- and 1074-nm Dual-Wavelength Nd:YAG Laser Using a Fabry–Perot Band-pass Filter as Output Mirror," IEEE Photonics J. **6**, 1–6 (2014).
52. Z. Lin, X. Huang, J. Lan, Y. Cheng, Y. Wang, B. Xu, H. Xu, and Z. Cai, "Efficient and Compact Diode-Pumped Nd:YAG Lasers at 1073 and 1078 nm," IEEE Photonics J. **8**, 1–8 (2016).
53. G. Shayeganrad and L. Mashhadi, "Dual-wavelength CW diode-end-pumped a-cut Nd:YVO_4 laser at 1064.5 and 1085.5 nm," Appl. Phys. B **111**, 189–194 (2013).
54. X. Wang, Z. Wang, Y. Bu, L. Chen, G. Cai, W. Huang, Z. Cai, and N. Chen, "Power-ratio tunable dual-wavelength laser using linearly variable Fabry–Perot filter as output coupler," Appl. Opt. **55**, 879–883 (2016).
55. G. Shayeganrad, Y.-C. Huang, and L. Mashhadi, "Tunable single and multiwavelength continuous-wave c-cut Nd:YVO_4 laser," Appl. Phys. B **108**, 67–72 (2012).
56. T. Waritanant and A. Major, "Dual-Wavelength CW Operations at 1064.1 & 1073.1 nm and 1064.1 & 1085.3 nm of Nd:YVO_4 Laser," Appl. Phys. B **124**, 87 (2018).
57. L. Chen, X. Xu, Z.Wang, D. Li, Haohai Yu, J. Xu, S. Zhuang, L. Guo, Y. Zhao, and X. Xu, "Efficient dual-wavelength operation of Nd:LYSO laser by diode pumping aimed toward the absorption peak," Chinese Opt. Lett. **9**, 071403–071403 (2011).
58. T. Jensen, V. G. Ostroumov, J.-P. Meyn, G. Huber, A. I. Zagumennyi, and I. A. Shcherbakov, "Spectroscopic characterization and laser performance of diode-laser-pumped Nd: $GdVO_4$," Appl. Phys. B **58**, 373–379 (1994).

59. P. A. Studenikin, A. I. Zagumennyi, Y. D. Zavartsev, P. A. Popov, and I. A. Shcherbakov, "$GdVO_4$ as a new medium for solid-state lasers: some optical and thermal properties of crystals doped with Cd^{3+}, Tm^{3+}, and Er^{3+} ions," Quantum Electron. **25**, 1162–1165 (1995).
60. H. Zhao, K. Sukhoy, I. T. Lima Jr., and A. Major, "Generation of green second harmonic with 60% conversion efficiency from a Q-switched microchip laser in MgO:PPLN crystal," Laser Phys. Lett. **9**, 355–358 (2012).
61. M. Nadimi, T. Waritanant, and A. Major, "Discrete multi-wavelength tuning of a continuous wave diode-pumped Nd:$GdVO_4$ laser," Laser Phys. Lett. **15**, 055002 (2018).
62. M. Nadimi, T. Waritanant, and A. Major, "Passively mode-locked high power Nd:$GdVO_4$ laser with direct in-band pumping at 912 nm," Laser Phys. Lett. **15**, 15001 (2018).
63. D. Sangla, M. Castaing, F. Balembois, and P. Georges, "Highly efficient Nd:YVO_4 laser by direct in-band diode pumping at 914 nm," Opt. Lett. **34**, 2159–2161 (2009).
64. T. Waritanant and A. Major, "Thermal lensing in Nd:YVO_4 laser with in-band pumping at 914 nm," Appl. Phys. B **122**, 135 (2016).
65. R. C. Talukder, Md. Z. E. Halim, T. Waritanant, and A. Major, "Multiwatt continuous wave Nd:KGW laser with hot-band diode pumping," Opt. Lett. **41**, 3810–3812 (2016).
66. S. Manjooran, P. Loiko, A. Major, "A discretely tunable dual-wavelength multi-watt Yb: CALGO laser," Appl. Phys. B **124**, 13 (2018).
67. S. Ghanbari and A. Major, "High power continuous-wave dual-wavelength Alexandrite laser," Laser Phys. Lett. **14**, 105001 (2017).
68. H. Zhao, A. Major, "Orthogonally polarized dual-wavelength Yb:KGW laser induced by thermal lensing," Appl. Phys. B 122, 163–169 (2016).

69. H. Zhao, A. Major, “Dynamic characterization of intracavity losses in broadband quasi-three-level lasers,” Opt. Express **22**, 26651–26658 (2014).

70. S. Ghanbari and A. Major, “High power continuous wave Alexandrite laser with green pump,” Laser Phys. **26**, 75001 (2016).

71. R. Akbari, A. Major, “High-power diode-pumped Kerr-lens mode-locked bulk Yb:KGW laser,” Appl. Opt. **56**, 8838–8844 (2017).

72. S. Ghanbari, R. Akbari, A. Major, “Femtosecond Kerr-lens mode-locked Alexandrite laser,” Opt. Express **24**, 14836–14840 (2016).

73. S. Ghanbari, K. A. Fedorova, A. B. Krysa, E. U. Rafailov, and A. Major, “Femtosecond Alexandrite laser passively mode-locked by an InP/InGaP quantum-dot saturable absorber,” Opt. Lett. **43**, 232–234 (2018).

74. B. Wu, P. Jiang, D. Yang, T. Chen, J. Kong, and Y. Shen, “Compact dual-wavelength Nd:$GdVO_4$ laser working at 1063 and 1065 nm,” Opt. Express **17**, 6004–6009 (2009).

Chapter 6 – Passively mode-locked high power Nd:$GdVO_4$ laser with direct in-band pumping at 912 nm[1]

Diode-pumped passively mode-locked solid-state lasers with high average power and good beam quality have applications in various areas such as industrial manufacturing [1], nonlinear frequency conversion [2-8], spectroscopy [9-11], and microscopy [12-14]. Recent efforts of power scaling of ultrashort pulse lasers included Yb-ion and Nd-ion doped lasers [15-19]. However, designing of a high power, high efficiency ML laser is a very challenging task mainly due to the thermal effects in the gain medium [20-22].

In chapter 4, we demonstrated a high power CW Nd:$GdVO_4$ laser with excellent beam quality using in-band diode pumping at 912 nm [23]. It was shown that the effect of thermal lensing strength was around two times lower when compared to the Nd:$GdVO_4$ laser with traditional 808 nm pumping or even Nd:YVO_4 laser with 914 nm pumping. Therefore, extending this promising pumping approach from the CW to the ML regime with Nd:$GdVO_4$ laser crystals is very attractive from the power scaling point of view and is the topic of the present work. This chapter consists of two main parts: Part 1 is an introduction about the technique of mode locking. Part 2 describes a

[1] Part 2 of this chapter contains material from [M. Nadimi, T. Waritanant, and A. Major, *"Passively mode-locked high power Nd:$GdVO_4$ laser with direct in-band pumping at 912 nm,"* Laser Phys. Lett. 15, 15001 (2018)].

semiconductor saturable absorber mirror mode-locked 1063 nm Nd:$GdVO_4$ laser in-band diode-pumped at the new wavelength of 912 nm.

6.1 Mode locking

Mode locking technique is usually implemented to produce ultrashort pulses of light. In a laser cavity with length *L*, under the continuous-wave operation, many discrete longitudinal modes are allowed to oscillate with a frequency interval $\Delta\nu=c/2L$, where *c* is the speed of light. The possible oscillating frequencies are shown in Fig. 6-1.

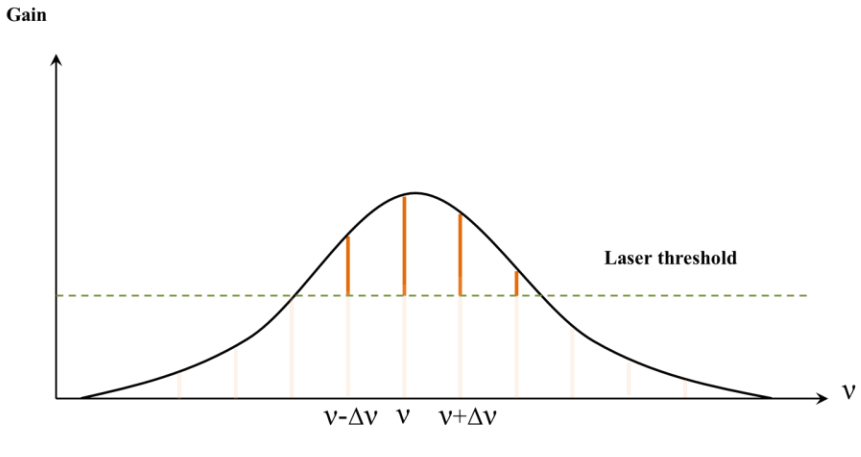

Fig. 6-1. Oscillating laser modes within the gain spectrum of a laser medium.

The term mode locking refers to “locking” of the laser longitudinal modes in phase in a way so that they can interfere constructively and form very short pulses of light. Without mode locking, these longitudinal modes have no well-defined phase relationship. The electric field amplitude of the laser output beam is an average of all allowed oscillating modes and it has a temporal shape as shown in Fig. 6-2-a. However, if all allowed modes have a fixed phase relationship then a constructive superposition of electric fields at a common point within the resonator can be achieved [24]. This phenomenon finally forms an intense ultrashort laser pulse in a cavity as shown in Fig. 6-2-b.

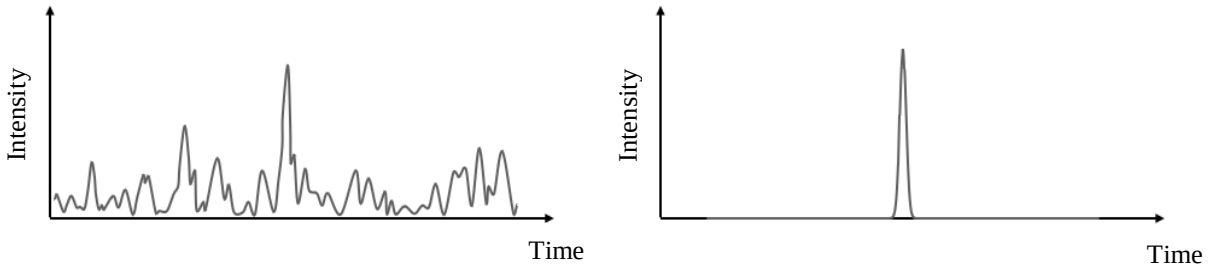

(a) (b)

Fig. 6-2. Mode locking effect in time domain. (a) Signal emitted from non-mode-locked lasers (signal has a characteristics of thermal noise). (b) Signal structure of an ideally mode-locked laser (signal has characteristics of a Gaussian pulse) [24].

6.1.1 Active and passive mode locking

Generally, in order to achieve mode locking in a laser system, an optical element with optical loss modulation capabilities should be introduced into the laser cavity. This will provide short moments when the net gain of the active medium becomes positive. This phenomenon is schematically demonstrated in Fig. 6-3. Usually, mode locking techniques can be divided into two main categories known as active mode locking and passive mode locking. In active mode locking, the periodic loss is typically introduced into the system via acousto-optic or electro-optic modulator. An externally applied electrical driving signal is typically used to modulate either the amplitude or the phase of the modes. If the modulation frequency is synchronized with the laser cavity roundtrip, then picosecond pulses can be obtained. In passive mode locking, the periodic loss is typically introduced into the laser cavity via passive optical elements such as semiconductor saturable absorber mirror (SESAM) or Kerr medium, in which the loss modulation is typically controlled by the intensity of the laser pulse itself. The passive optical elements can modulate the resonator losses much faster than any acousto-optic or electro-optic modulator. Therefore, passive mode locking technique enables the generation of much shorter pulses than the active mode locking technique. In this research, SESAM was used to produce short picosecond pulses.

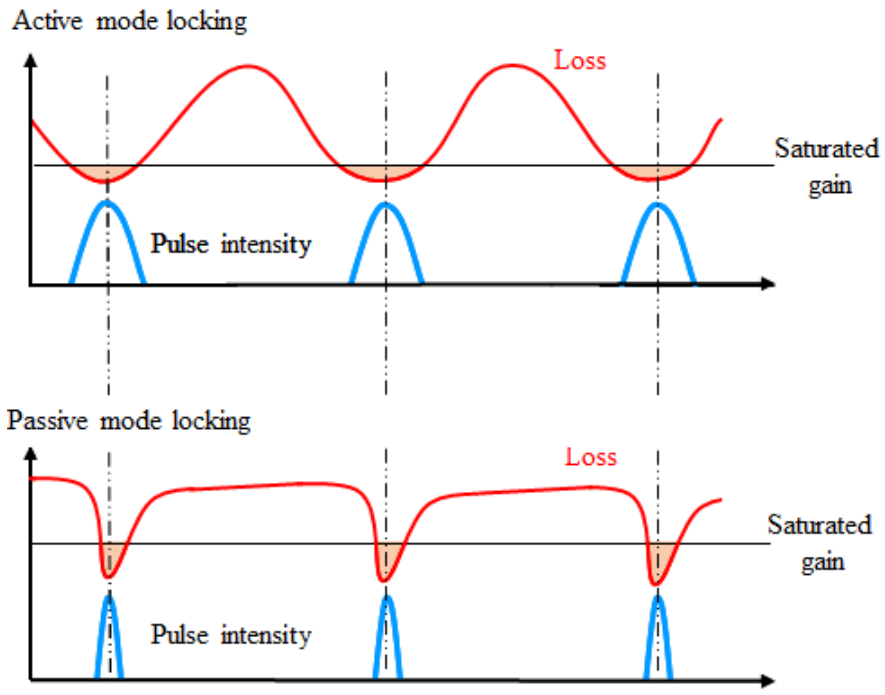

Fig. 6-3. Loss modulation: Active and passive mode locking [25].

6.1.2 Mode locking with semiconductor saturable absorber mirror

A semiconductor saturable absorber mirror typically consists of an InGaAs or GaAs quantum well and a Bragg reflector on a semiconductor substrate as demonstrated in Fig. 6-4. The quantum well acts as a saturable absorber and the Bragg reflector can act as an HR mirror. In the saturable absorber low intensity light will be absorbed and excite electrons from the valence band to the conduction band. However, at high light intensity, the valence band will be depleted and as a result no absorption happens (i.e. saturation of the absorption takes place). This situation will continue until the carriers relax back to the lower energy level. Therefore, by inserting a SESAM into the laser cavity, the low intensity light will be blocked while the high intensity light can circulate throughout the cavity with minimum loss. This will correspond to the transition of a laser from the CW regime (low intensity) to the mode-locked one with high intensity light pulses because pulses will see a lower loss (i.e. higher gain) in the cavity.

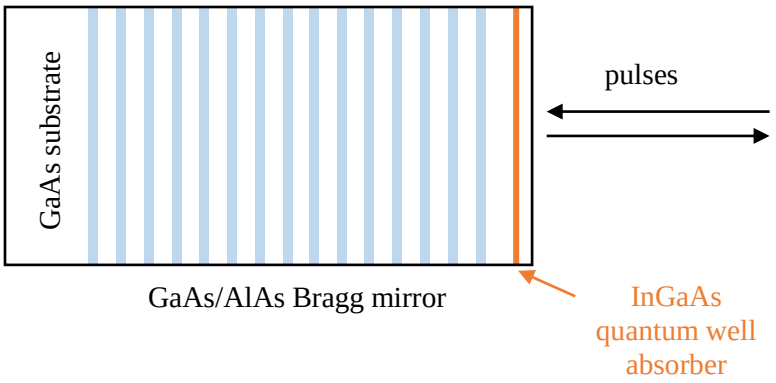

Fig. 6-4. Structure of a SESAM [26]

6.2 Passively mode-locked high power Nd:$GdVO_4$ laser with direct in-band pumping at 912 nm

6.2.1 Introduction

SESAM mode locking is a well-known passive technique to generate ultrashort laser pulses from Nd-ion and Yb-ion doped laser materials [27-32]. The first SESAM mode-locked Nd:$GdVO_4$ laser was reported in 2003 with the 600 mW of average output power and 8 ps pulse duration [33]. Since then various groups reported on higher output power ML Nd:$GdVO_4$ lasers under the standard 808 nm pumping [34-36]. In 2007, the output power as high as 6.5 W was reported with the optical-to-optical efficiency of 32.5%, pulse duration of 6.2 ps and a repetition rate of ~110 MHz [37]. About a decade later, Lin et al. demonstrated a 37 W, 19.3 ps Nd:$GdVO_4$ laser using a σ-polarized in-band pumping at 880 nm [38]. The reported optical-to-optical efficiency was 51%. Despite the active research associated with mode locking of the Nd:$GdVO_4$ and Nd:YVO_4 lasers, there are only two reports available on their performance under the ~912/914 nm pumping. The first work was a Nd:$Gd_{0.6}Y_{0.4}VO_4$ laser with an optical-to-optical efficiency of 27% and slope efficiency of 44% [39], where the low efficiency was due to the non-optimal mode-matching condition between the laser and pump beams. The second work recently reported on a ML

Nd:YVO_4 laser with the highest efficiency among the Nd-doped lasers in the ML regime [19]. The laser generated an average output power of 6.7 W with a slope efficiency of 77.1% and pulse width of 16 ps. To the best of our knowledge, there has been no report so far on a ML Nd:$GdVO_4$ laser diode-pumped at 912 nm. In this section we addressed this issue and studied the possibility of high power operation of the SESAM ML Nd:$GdVO_4$ laser under the 912 nm diode pumping.

6.2.2 Experimental setup

The experimental setup is shown in Fig. 6-5. The cavity was built around the previously used 20-mm-long 1.5 at. % doped a-cut Nd:$GdVO_4$ crystal. The laser crystal was wrapped in indium foil and water-cooled at 16℃ on its top and bottom surfaces. The system was pumped by a fiber-coupled laser diode operating around 912 nm (105 μm core diameter, NA = 0.22). The pump radiation produced a spot diameter of 525 μm at the center of the crystal.

The cavity consisted of 5 mirrors: a reflective SESAM as one of the end mirrors, a dichroic mirror with antireflection coating at 912 nm and high-reflection coating at 1063 nm and two curved mirrors (M2, M3) with radii of curvature of 400 and 500 mm, respectively. The distances L1, L2, L3, and L4 were 31.5, 48, 46.5, and 44 cm, respectively. The cavity design was such that at high power operation, the effect of thermal lensing on mode size variation in the crystal and on the SESAM was reduced [40]. The laser beam spot diameter at the center of crystal was ~525 μm at the maximum absorbed pump power. At the same time, the beam radius on the SESAM was around 180 μm which resulted in a proper fluence to achieve stable continuous-wave ML without multi-pulse instabilities [41] or any damage to the SESAM. The transmission of output coupler was optimized to get the highest output power and was 15% in the mode locking experiments.

The SESAM (BATOP GmbH) that was used in this work had a modulation depth of 1.2%, saturation fluence of 90 μJ/cm^2, non-saturable loss of 0.8% and a relaxation time constant of ~10 ps.

Furthermore, a 6 GHz digital storage oscilloscope (Tektronix, TDS6604) with a fast photodetector were used to monitor the mode-locked pulse train. Pulse duration was measured using an intensity autocorrelator (Femtochrome Research, FR-103XL) and a charge coupled device (CCD) camera was used to characterize the laser beam quality factor.

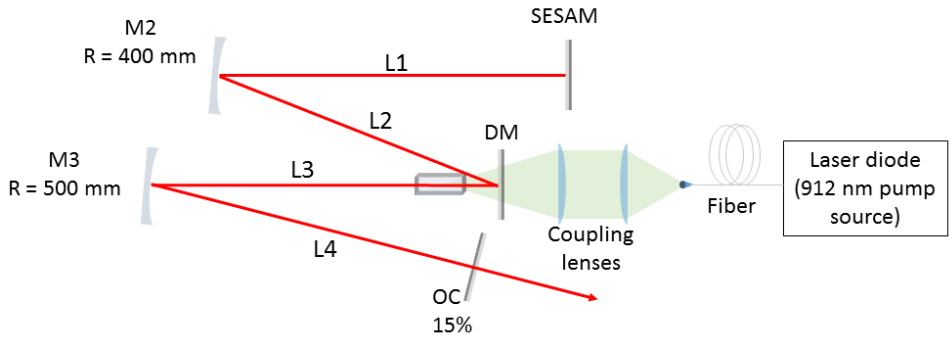

Fig. 6-5. Experimental setup of the mode-locked Nd:$GdVO_4$ laser.

6.2.3 Results and discussion

Fig. 6-6 shows the output power versus the absorbed pump power of the Nd:$GdVO_4$ laser. Below 10 W of the pump power the laser operated in the CW regime. Further pump power increase resulted in the Q-switched mode-locked operation (QSML). Above 15 W of pump power (6.7 W of output power), stable mode-locked operation was observed. Such transition from the CW to the ML regime is typical for the SESAM mode-locked solid-state lasers [27]. The highest output power of 10.14 W was obtained at 20.44 W of the absorbed pump power which corresponds to the optical-to-optical efficiency of 49.6%. The slope efficiency in the ML regime was calculated to be 67.4%. The overall laser slope efficiency (taking into account CW, QSML and ML regimes) was

51.3%. This can be explained by the dynamic influence of thermal lensing and the design of the laser resonator which was optimized for high power operation.

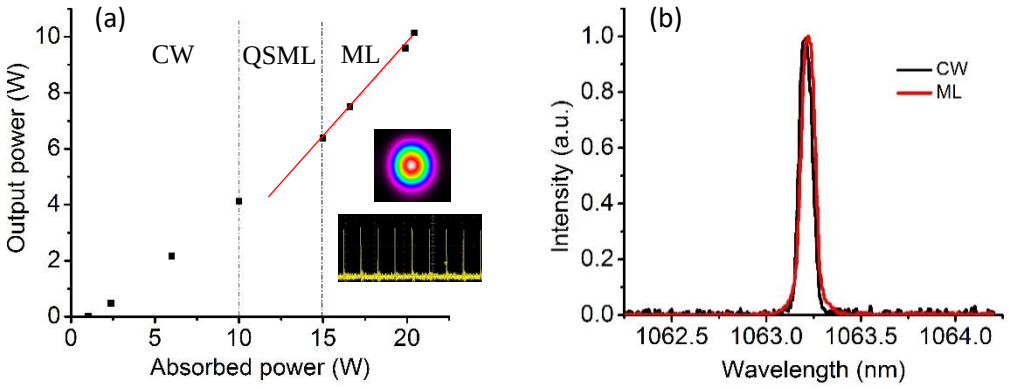

Fig. 6-6. (a) Average output power of the Nd:$GdVO_4$ laser versus the absorbed pump power. Insets: beam shape at 10.14 W of output power and ML pulse train in a 95 ns long time window. (b) Laser output spectra in the CW and ML operation regimes.

Taking into account the slope efficiency of our system, it is clear that the maximum output power was limited by the available pump power instead of the conventional thermal lensing problems which result in output power roll-off. Indeed, a more powerful pumping source, longer crystal or multi-pass pumping scheme can be used to power scale the output power in our case.

The laser produced an excellent output beam shape (as shown in the inset of Fig. 6-6-a) and the M^2 parameter was measured to be 1.2 at full output power. The mode-locked pulse train had a period of ~11.7 ns and it is shown in the inset of Fig. 6-6-a.

The optical spectra of the laser output in the CW and ML regimes were measured and are displayed in Fig. 6-6-b. In both cases the FWHM was ~0.08 nm at the central wavelength of ~1063.2 nm.

The pulse width of the ML laser output at full output power was measured by an intensity autocorrelator (AC). The AC trace is shown in Fig. 6-7-a and the pulse width was measured to be 16 ps assuming a $sech^2$- shaped pulses. Fig. 6-7-b shows the radio frequency (RF) spectrum of the

ML pulse train, where the signal level was 40 dBm above the noise level thus confirming the stable mode locking without any signs of multi-pulsing instabilities. Considering the pulse duration of 16 ps and repetition rate of 85.2 MHz, the maximum pulse peak power and energy can be calculated to be 7.44 kW and 119 nJ, respectively.

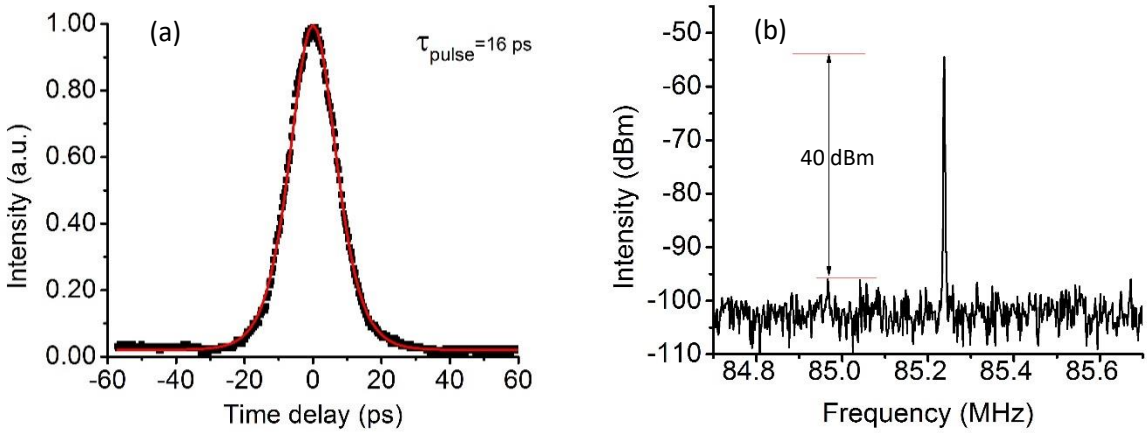

Fig. 6-7. (a) The intensity autocorrelation trace (dots) and *sech*^{2} fit (solid line) of the generated pulses. (b) Radio frequency spectrum of the Nd:$GdVO_4$ laser pulse train with resolution bandwidth of 1 kHz.

Comparing to the other available pumping wavelengths for the Nd:$GdVO_4$ crystal, the new pumping scheme at 912 nm results in the lowest quantum defect [23]. This allowed us to lower the effect of thermal lensing and maximize the laser efficiency. The experimentally obtained output power and optical-to-optical efficiency in our case are far more superior in comparison with all of the available reports for conventional 808 nm pumped Nd:$GdVO_4$ lasers [33, 35-37], where significant thermal lensing limited output powers to well below 10 W and the optical-to-optical efficiency to ~30%. In addition, to the best of our knowledge, this is the highest average output power between all of the SESAM mode-locked Nd-doped solid-state lasers that were pumped around 912 nm [19, 30, 39]. In comparison with the recent 37 W mode-locked Nd:$GdVO_4$ laser with polarized pumping at 880 nm [38], the present work has a lower quantum defect and more

than an order of magnitude lower pumping threshold. At the same time, it should be noted that polarizing of the pump radiation from the generally unpolarized output of the fiber-coupled diode modules results in a loss of about half of the total available pump power. Taking this into account, the claimed optical-to-optical efficiency of 51% should be reduced by a factor of two, thus making it comparable to the standard diode-pumping at 808 nm which is twice lower than in our experiment. Nevertheless, the produced output power of 37 W with less than optimal quantum defect (i.e. higher thermal lensing) points out that pumping at 912 nm is a very promising approach for further power scaling of the Nd:$GdVO_4$ and other Nd-ion based lasers.

6.2.4 Conclusion

In summary, we have demonstrated the first SESAM mode-locked 1063 nm Nd:$GdVO_4$ laser in-band diode-pumped at 912 nm. The developed laser system generated 10.14 W of average output power with the pulse duration of 16 ps, repetition rate of 85 MHz, optical-to-optical efficiency of ~49.6 % and slope efficiency of 67.4% in the mode-locked regime. To the best of our knowledge, this is the highest average output power ever obtained for the mode-locked Nd-doped lasers that were pumped around 912 nm. Considering the fact that the output power of our laser was limited only by the available pump power, we believe that this result opens a new avenue for power scaling of the mode-locked and continuous-wave lasers based on the Nd-ion doped crystals in general and on Nd:$GdVO_4$ crystal in particular.

References

1. K. Sugioka and Y. Cheng, “Ultrafast lasers—reliable tools for advanced materials processing,” Light Sci. Appl. **3,** e149 (2014).

2. H. Zhao, I. T. Lima, and A. Major, “Near-infrared properties of periodically poled $KTiOPO_4$ and stoichiometric MgO-doped $LiTaO_3$ crystals for high power optical parametric oscillation with femtosecond pulses,” Laser Phys. **20**, 1404–1409 (2010).
3. I. T. Lima, V. Kultavewuti, and A. Major, “Phasematching properties of congruent MgO-doped and undoped periodically poled $LiNbO_3$ for optical parametric oscillation with ultrafast excitation at 1 μm,” Laser Phys. **20**, 270–275 (2010).
4. S. Manjooran, H. Zhao, I. T. Lima, and A. Major, “Phase-matching properties of PPKTP, MgO:PPSLT and MgO:PPcLN for ultrafast optical parametric oscillation in the visible and near-infrared ranges with green pump,” Laser Phys. **22**, 1325–1330 (2012).
5. R. Akbari and A. Major, “Optical, spectral and phase-matching properties of BIBO, BBO and LBO crystals for optical parametric oscillation in the visible and near-infrared wavelength ranges,” Laser Phys. **23**, 35401 (2013).
6. A. Major, D. Sandkuijl, and V. Barzda, “Efficient frequency doubling of a femtosecond Yb:KGW laser in a BiB_3O_6 crystal,” Opt. Express **17**, 12039–12042 (2009).
7. A. Major, J.S. Aitchison, P.W.E. Smith, N. Langford, A.I. Ferguson, “Efficient Raman shifting of high-energy picosecond pulses into the eye-safe 1.5 μm spectral region using a $KGd(WO_4)_2$ crystal,” Opt. Lett. **30**, 421–423 (2005).
8. A. Major, K. Sukhoy, H. Zhao, and I. T. Lima Jr, “Green sub-nanosecond microchip laser based on BiBO crystals,” Laser Physics **21**, 57–60 (2011).
9. A. Major, F. Yoshino, J. S. Aitchison, P. W. E. Smith, E. Sorokin, and I. T. Sorokina, “Ultrafast nonresonant third-order optical nonlinearities in ZnSe for photonic switching at telecom wavelengths,” Appl. Phys. Lett. **85**, 4606 (2004).

10. I. P. Nikolakakos, A. Major, J. S. Aitchison, and P. W. E. Smith, “Broadband Characterization of the Nonlinear Optical Properties of Common Reference Materials,” IEEE J. Sel. Top. Quantum Electron. **10**, 1164–1170 (2004).
11. A. Major, J. S. Aitchison, P. W. E. Smith, F. Druon, P. Georges, B. Viana, and G. P. Aka, “Z-scan measurements of the nonlinear refractive indices of novel Yb-doped laser crystal hosts,” Appl. Phys. B **80**, 199–201 (2005).
12. D. Sandkuijl, R. Cisek, A. Major, and V. Barzda, “Differential microscopy for fluorescence-detected nonlinear absorption linear anisotropy based on a staggered two-beam femtosecond Yb:KGW oscillator,” Biomed. Opt. Express **1**, 895-901 (2010).
13. A. Major, R. Cisek and V. Barzda, “Development of diode-pumped high average power continuous-wave and ultrashort pulse Yb:KGW lasers for nonlinear microscopy,” Proc. SPIE 6108, 61080Y (2006).
14. L. B. Mostaço-Guidolin, A. C-T. Ko, D. P. Popescu, M. S. D. Smith, E. K. Kohlenberg, M. Shiomi, A. Major, M. G. Sowa, “Evaluation of texture parameters for the quantitative description of multimodal nonlinear optical images from atherosclerotic rabbit arteries,” Physics in Medicine and Biology **56,** 5319-5334 (2011).
15. R. Akbari, H. Zhao, K. A. Fedorova, E. U. Rafailov, and A. Major, “Quantum-dot saturable absorber and Kerr-lens mode-locked Yb:KGW laser with >450 kW of peak power,” Opt. Lett. **41**, 3771–3774 (2016).
16. H. Zhao and A. Major, "Megawatt peak power level sub-100 fs Yb:KGW oscillators," Opt. Express **22**, 30425-30431 (2014).

17. S. Manjooran, and A. Major, “Generation of sub-50 fs pulses with >1.5 MW of peak power from a diode-pumped Yb:CALGO laser oscillator,” Conference on Lasers and Electro-Optics, **JTu5A.82** (2016).
18. R. Akbari, K. A. Fedorova, E. U. Rafailov and A. Major “Diode-pumped ultrafast Yb:KGW laser with 56 fs pulses and multi-100 kW peak power based on SESAM and Kerr-lens mode locking,” Appl. Phys. B **123** 123 (2017).
19. T. Waritanant and A. Major, “High efficiency passively mode-locked Nd:YVO_4 laser with direct in-band pumping at 914 nm,” Opt. Express **24**, 12851–12855 (2016).
20. T. Waritanant and A. Major, “Thermal lensing in Nd:YVO_4 laser with in-band pumping at 914 nm,” Appl. Phys. B **122**, 135 (2016).
21. P. Loiko, S. Manjooran, K. Yumashev, and A. Major, “Polarization anisotropy of thermal lens in Yb:$KY(WO_4)_2$ laser crystal under high-power diode pumping,” Appl. Opt. **56**, 2937– 2945 (2017).
22. H. Zhao and A. Major “A continuous wave Yb:KGW laser with polarization-independent pump absorption,” Laser Phys. **23,** 09500 (2013).
23. M. Nadimi, T. Waritanant, and A. Major, “High power and beam quality continuous-wave Nd:$GdVO_4$ laser in-band diode-pumped at 912 nm,” Photon. Res. **5**, 346–349 (2017).
24. W. Koechner, Solid-state Laser Engineering, 6th ed. (Springer, 2006).
25. U. Keller, “Recent developments in compact ultrafast lasers,” Nature **424**, 831–838 (2003).
26. R. Paschotta, “Encyclopedia of laser physics and technology.” [Online]. Available: https://www.rp-photonics.com/semiconductor_saturable_absorber_mirrors.html.
27. U. Keller, K. J. Weingarten, F. X. Kärtner, D. Kopf, B. Braun, I. D. Jung, R. Fluck, C. Hönniger, N. Matuschek, and J. Aus der Au, “Semiconductor saturable absorber mirrors (SESAM’s) for

femtosecond to nanosecond pulse generation in solid-state lasers," IEEE J. Sel. Top. Quantum Electron. **2**, 435-453 (1996).

28. T. Waritanant and A. Major, "Discretely selectable multiwavelength operation of a semiconductor saturable absorber mirror mode-locked Nd:YVO_4 laser," Opt. Lett. **42**, 3331–3334 (2017).
29. A. Major, V. Barzda, P. A. E. Piunno, S. Musikhin and U.J. Krull, "Development of femtosecond Yb:KGW laser for applications in optical DNA sensor technology," Proc. SPIE, **5969** 59690Q (2005).
30. Md. Z. E. Halim, R. C. Talukder, T. Waritanant, and A. Major, "Passive mode locking of a Nd:KGW laser with hot-band diode pumping," Laser Phys. Lett. **13**, 105003 (2016).
31. A. Major, L. Giniunas, N. Langford, A. I. Ferguson, D. Burns, E. Bente, and R. Danielius, "Saturable Bragg reflector-based continuous-wave mode locking of Yb:$KGd(WO_4)_2$ laser," J. Mod. Opt. **49**, 787-793 (2002).
32. A. Major, N. Langford, Th. Graf, D. Burns, and A.I. Ferguson, "Diode-pumped passively mode-locked Nd:$KGd(WO_4)_2$ laser with 1W average output power," Opt. Lett. **27**, 1478–1480 (2002).
33. B. Zhang, G. Li, M. Chen, Z. Zhang, and Y. Wang, "Passive mode locking of a diode-end-pumped Nd:$GdVO_4$ laser with a semiconductor saturable absorber mirror," Opt. Lett. **28**, 1829–1831 (2003).
34. J.-L. He, C.-K. Lee, J. Y. J. Huang, S.-C. Wang, C.-L. Pan, and K.-F. Huang, "Diode-pumped passively mode-locked multiwatt Nd:$GdVO_4$ laser with a saturable Bragg reflector," Appl. Opt. **42**, 5496–5499 (2003).
35. J. Kong, D. Y. Tang, S. P. Ng, B. Zhao, L. J. Qin, and X. L. Meng, "Diode-pumped passively mode-locked Nd:$GdVO_4$ laser with a GaAs saturable absorber mirror," Appl. Phys. B **79**, 203–206 (2004).

36. E. Wu, "Passive mode locking in a diode-pumped Nd:$GdVO_4$ laser with a semiconductor saturable absorber mirror," IEEE J. Quantum Electron. **40**, 505–508 (2004).

37. J. Y. Peng, B. S. Wang, Y. G. Wang, J. G. Miao, E. J. Hao, H. M. Tan, L. S. Qian, and X. Y. Ma, "High average power and short pulse duration continuous wave mode-locked Nd:$GdVO_4$ laser with a semiconductor absorber mirror," Laser Phys. **17**, 1033–1036 (2007).

38. H. Lin, J. Guo, P. Gao, H. Yu, and X. Liang, "High power, diffraction limited picosecond oscillator based on Nd:$GdVO_4$ bulk crystal with σ polarized in-band pumping," Opt. Express **24**, 13957–13962 (2016).

39. H. C. Liang, Y. J. Huang, P. Y. Chiang, and Y. F. Chen, "Highly efficient Nd:$Gd_{0.6}Y_{0.4}VO_4$ laser by direct in-band pumping at 914 nm and observation of self-mode-locked operation," Appl. Phys. B **103**, 637–641 (2011).

40. H. Mirzaeian, S. Manjooran, and A. Major, "A simple technique for accurate characterization of thermal lens in solid state lasers," Proc. SPIE **9288**, 928802 (2014).

41. C. Hönninger, R. Paschotta, F. Morier-Genoud, M. Moser, and U. Keller, "Q-switching stability limits of continuous-wave passive mode locking," J. Opt. Soc. Am. B. **16** 46-56 (1999).

Chapter 7 – Conclusions and future work

This thesis discussed the capabilities of Nd:$GdVO_4$ laser crystal for the generation of high power CW and short pulse laser radiation with in-band diode pumping at 912 nm.

Thermal lensing effect is the most important constraint in power scaling of the vanadate based crystals. Therefore, suitability of diode pumping at 912 nm for reduction of the thermal lensing effect in Nd:$GdVO_4$ laser was investigated both experimentally and by FEA simulation. The thermal lensing strength in Nd:$GdVO_4$ laser under 912 nm pumping was found to be around two times weaker when compared to the Nd:$GdVO_4$ laser with standard 808 nm pumping or Nd:YVO_4 laser with 914 nm pumping. These results confirm that the thermal conductivity of Nd:$GdVO_4$ crystal is higher than that of the Nd:YVO_4 crystal despite recent uncertainties on their true values. Therefore, due to lower thermal problems, the Nd:$GdVO_4$ crystal is recommended as a more attractive candidate for high power applications than the well-known Nd:YVO_4 crystal.

After thermal lensing evaluation, we built a 19.8 W CW Nd:$GdVO_4$ laser with low threshold, high efficiency and excellent beam quality. The previous maximum reported output power with similar pumping wavelength was 3.35 W. The results of this part of the research confirm that the diode pumping of the Nd:$GdVO_4$ crystal at 912 nm opens a way for further output power scaling. The developed high-power, high beam quality CW Nd:$GdVO_4$ laser is attractive for mode locking. Therefore, mode-locked operation was examined with SESAM and we were able generate 10.14 W of averaged output power at 1063 nm with the pulse width of 16 ps. To the best of our knowledge, this is not only the first SESAM mode-locked Nd:$GdVO_4$ laser under 912 nm diode pumping but also the highest average output power between all of the SESAM mode-locked Nd-doped solid-state lasers that were pumped at similar wavelength.

During the development of the laser system, discrete CW multi-wavelength operation (1071/1083/1086 nm) and CW dual-wavelength operation within $^4F_{3/2}$–$^4I_{11/2}$ transition were demonstrated based on a simple approach. The former is desirable for optical pumping of helium or similar atomic studies and the latter is attractive in THz generation applications.

All of the aforementioned demonstrations reveal and confirm the capabilities of the Nd:$GdVO_4$ crystal for generation of high power CW and short pulses based upon efficient and low cost approaches.

We believe that the performance of Nd:$GdVO_4$ lasers at 1063 nm in both CW and ML regimes in this work was limited by the available pump source. The output power can be scaled by using a more powerful pumping source to compensate for the lower absorption coefficient of Nd:$GdVO_4$ crystal at 912 nm as compared to the other pump wavelengths. However, further optimization of laser cavity would be necessary as at high powers the thermal lensing strength would be increased. The numerical calculations provided in chapter 3 would be helpful for such a system design. In addition, when dealing with the mode locking regime, the fluence (pulse energy per unit area) on the SESAM should be chosen in a proper manner to achieve stable mode locking without multi-pulse instabilities or damages to the absorber.

Another interesting topic for the future research is investigation of generation of picosecond pulses from the Nd:$GdVO_4$ lasers at 1071 nm and 1083 nm and their frequency conversion.